AD-A053 289 BATTELLE COLUMBUS LABS OHIO F/G 11/6
INVESTIGATION OF REJUVENATION OF FATIGUE DAMAGE IN TI-6AL-4V.(U)
JUL 77 A H CLAUER, B N LEIS, R B LOVE F33615-76-C-5100
UNCLASSIFIED AFML-TR-77-107 NL

1 OF 2
AD A053289

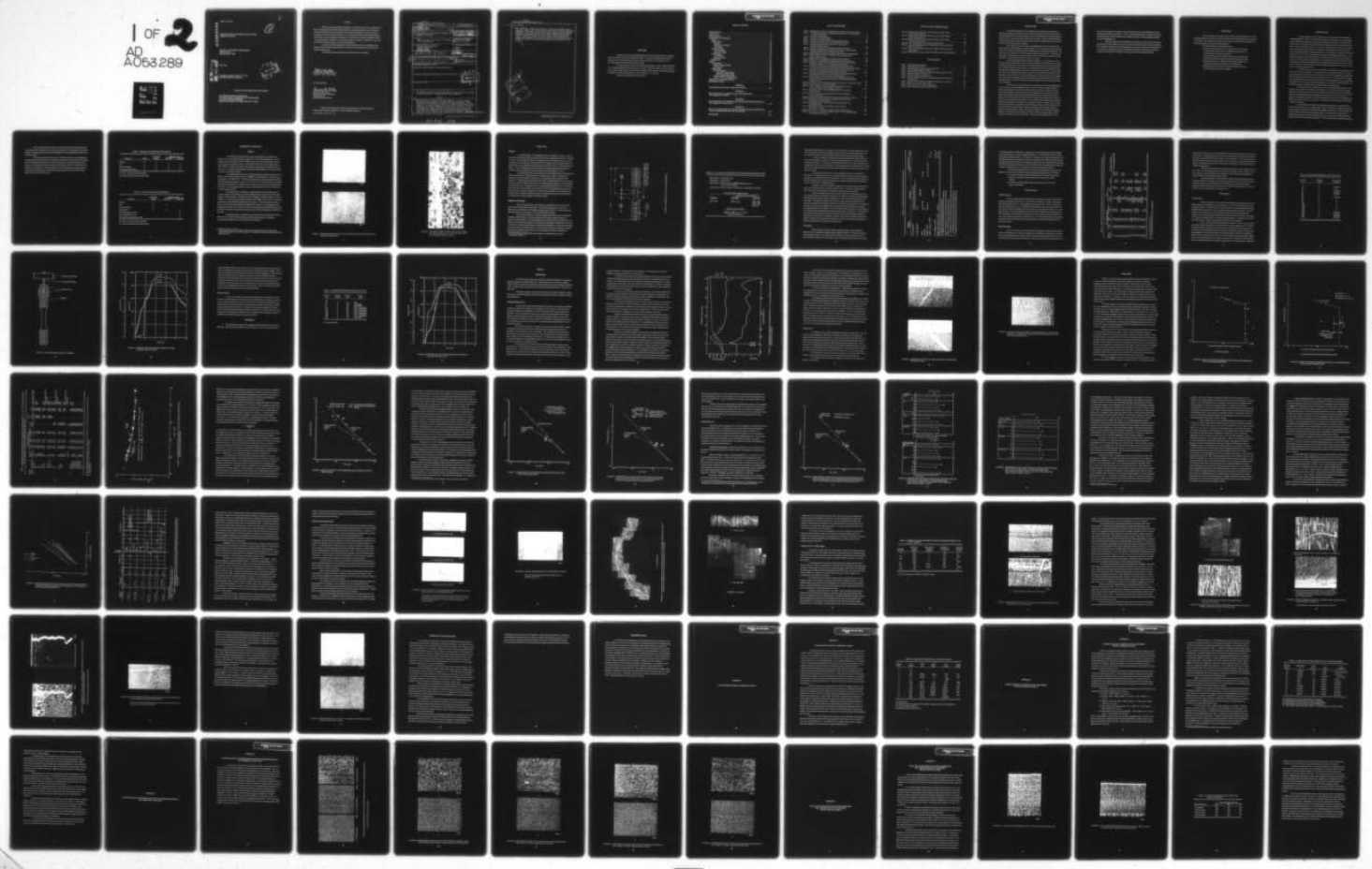

AFML-TR-77-107

INVESTIGATION OF REJUVENATION OF FATIGUE DAMAGE IN Ti-6Al-4V

BATTELLE- COLUMBUS LABORATORIES
505 King Avenue
Columbus, Ohio 43201

JULY 1977

TECHNICAL REPORT AFML-TR-77-107
INTERIM REPORT FOR PERIOD

AIR FORCE MATERIALS LABORATORY
AIR FORCE WRIGHT AERONAUTICAL LABORATORIES
AIR FORCE SYSTEMS COMMAND
WRIGHT-PATTERSON AIR FORCE BASE, OHIO 45433

NOTICE

When Government drawings, specifications, or other data are used for any purpose other than in connection with a definitely related Government procurement operation, the United States Government thereby incurs no responsibility nor any obligation whatsoever; and the fact that the government may have formulated, furnished, or in any way supplied the said drawings, specifications, or other data, is not to be regarded by implication or otherwise as in any manner licensing the holder or any other person or corporation, or conveying any rights or permission to manufacture, use, or sell any patented invention that may in any way be related thereto.

This report has been reviewed by the Information Office (OI) and is releaseable to the National Technical Information Service (NTIS). At NTIS, it will be available to the general public, including foreign nations.

This technical report has been reviewed and is approved for publication.

Attwell M. Adair, Project Engineer

For the Commander:

Norman M. Tallan, Chief
Processing and High Temperature
Materials Branch
Metals and Ceramics Division

Copies of this report should not be returned unless return is required by security considerations, contractual obligations, or notice on a specific document.

AIR FORCE/56780/10 February 1978 — 300

Unclassified

SECURITY CLASSIFICATION OF THIS PAGE (When Data Entered)

(19) REPORT DOCUMENTATION PAGE

READ INSTRUCTIONS BEFORE COMPLETING FORM

1. REPORT NUMBER (18) AFML-TR-77-107	2. GOVT ACCESSION NO.
3. RECIPIENT'S CATALOG NUMBER	
4. TITLE (and Subtitle) (6) Investigation of Rejuvenation of Fatigue Damage in Ti-6Al-4V	5. TYPE OF REPORT & PERIOD COVERED (9) Interim Report, ~~for period~~ 1 Jan 76-15 Mar 77
6. PERFORMING ORG. REPORT NUMBER	
7. AUTHOR(s) Clauer, A.H., Leis, B.N.; Love, R.B.; Seifert, D.A.; and Hanes, H.D.	8. CONTRACT OR GRANT NUMBER(s) (15) F33615-76-C-5100 per
9. PERFORMING ORGANIZATION NAME AND ADDRESS Battelle Memorial Institute Columbus Laboratories 505 King Avenue Columbus, OH 43221	10. PROGRAM ELEMENT, PROJECT, TASK AREA & WORK UNIT NUMBERS ILIR0078 61101F
11. CONTROLLING OFFICE NAME AND ADDRESS (16) ILIR (17) 00	12. REPORT DATE (11) July 1977
	13. NUMBER OF PAGES (12) 99p.
14. MONITORING AGENCY NAME & ADDRESS (if different from Controlling Office) (10) A. H. Clauer, B. N. Leis, R. B. Love, D. A. Seifert H. D. Hanes	15. SECURITY CLASS. (of this report) Unclassified
	15a. DECLASSIFICATION/DOWNGRADING SCHEDULE

16. DISTRIBUTION STATEMENT (of this Report)

Approved for public release; distribution unlimited.

DDC RECEIVED APR 27 1978 F

17. DISTRIBUTION STATEMENT (of the abstract entered in Block 20, if different from Report)

18. SUPPLEMENTARY NOTES

19. KEY WORDS (Continue on reverse side if necessary and identify by block number)

Hot Isostatic Processing, HIP, Fatigue Damage, Fatigue Rejuvenation, Coating, Titanium-6 Aluminum - 4 Vanadium, Physical Vapor Deposition

BETA

20. ABSTRACT (Continue on reverse side if necessary and identify by block number)

The feasibility of restoring the fatigue properties of fatigue damaged Ti-6Al-4V using hot isostatic processing (HIP) was investigated. Ti-6Al-4V specimens in the (β) solution treated and over-aged condition were fatigue damaged to two levels of damage: just before crack initiation and after crack initiation. The fatigue specimens were coated with a Ti-6Al-4V coating after damaging to isolate the surface cracks from the HIP atmosphere and cause them to be closed during HIP. Metallographic examination showed the cracks were not all bridged by the coating and these unbridged cracks did not

(Continued) → over

DD FORM 1 JAN 73 1473 EDITION OF 1 NOV 65 IS OBSOLETE

SECURITY CLASSIFICATION OF THIS PAGE (When Data Entered)

407 080 JOB

20. (Continued)

close during HIP. Evidence was obtained to indicate that fatigue cracks which were bridged by the coating could be closed and bonded under appropriate conditions. The results of the fatigue damage, coating and HIP experiments indicated that the total fatigue life of fatigue damaged specimens could be extended by coating and HIP, including specimens having surface fatigue cracks. Although the feasibility of the process has been demonstrated, further work to explore other coating procedures and more extensive fatigue testing is required to define the full potential and limitations of the process.

FOREWORD

This report was prepared by Battelle Memorial Institute, Columbus Division, Columbus, Ohio, under USAF Contract No. F33615-76-C-5100. The contract was administered under the direction of the Air Force Materials Laboratory, Wright-Patterson Air Force Base, Ohio, with Mr. Attwell M. Adair (AFML/LLM) as Project Engineer.

The work described in this report was carried out between 1 January 1976 and 15 March 1977. Principal researchers on the project were Dr. Allan H. Clauer, Dr. Brian N. Leis, Mr. R. Bruce Love, and Mr. David A. Seifert and were under the direction of Mr. Hugh D. Hanes, Program Manager. Contributions by AFML were made by Mr. A. M. Adair and Dr. H. A. Lipsitt.

This report was submitted on 20 April 1977.

TABLE OF CONTENTS

LIST OF ILLUSTRATIONS

LIST OF ILLUSTRATIONS (Continued)

LIST OF TABLES

INTRODUCTION

Hot isostatic processing (HIP) is undergoing rapid development as a materials processing method because of its ability to rapidly close internal porosity and bond interior surfaces. HIP accomplishes this by exerting high pressure at an elevated temperature to encourage creep and diffusion closure of voids and diffusion bonding of the interfaces. Although originally developed for diffusion bonding, its use has expanded to rapidly densifying powder metallurgy preforms, and closing shrinkage and gas porosity in castings.

More recently, the concept has been extended to closure of strain induced cavities originating from elevated temperature creep and fatigue.[1-3] In these cases the creep damage, and under certain conditions the fatigue damage, develops primarily as intergranular cavities and cracks in the interior of the material. This type of damage is readily removed by HIP. The original creep properties of the treated material are largely restored,[1,3] and the fatigue properties are partially restored[2], i.e., these material properties have been rejuvenated.

Strain induced cavitation and cracking are important in hot path components in aircraft gas turbines, such as blades or buckets. However, a possibly more important form of damage is surface-connected cracks. These may be either pre-existing cracks of a size below the detection level, or fatigue cracks initiated during service. In either case, the lifetime of components subject to predominantly fatigue damage is limited by the cyclic growth of these cracks. One such component is disks. The replacement cost of disks is large, but the consequences of a disk failure are so dangerous to aircraft and human life that the design life of a disk is a small fraction of its possible life. If a procedure for healing all preexisting or fatigue induced surface cracks could be devised, the allowable lifetime of disks could probably be extended substantially with attendant savings in cost and materials.

The healing of surface-connected cracks and restoration of the original fatigue properties is a much more challenging problem than the removal of internal cavitation because the problem areas appear to be more difficult to solve. Firstly, to enhance the ability to bond the crack surfaces together, an effective surface cleaning technique must be devised which ideally would reach into narrow, deep cracks to remove surface films and compounds such as oxides. Secondly, a means of blocking off the crack from the atmosphere is required so that the external pressure will act to squeeze the crack closed. For this purpose a sound coating able to bridge and seal all surface cracks must be developed. If the coating is to remain on the part when it reenters service, its presence must not impair the original properties of the part, and if the coating is to be removed before the part is placed back in service, the coating must be removable without impairing the original properties. Thirdly, if the material's properties are significantly decreased by changes in its microstructure incurred by the HIP cycle, the alloy must be amenable to reheat-treatment to restore the original microstructure. Fourthly, if alloy depleted zones form in the

vicinity of the crack due to oxidation or other compound formation, these deficiencies must be corrected or their effect accounted for. Fifthly, a final finishing procedure to restore the original surface dimensions, finish, or properties, e.g., hardness, chemistry, must be developed to prepare the part for subsequent use.

While the problems and risks associated with healing of surface-connected cracks and rejuvenation of fatigue properties are large, the potential economic and materials benefits are also large. Successful rejuvenation would conceivably not only enable used disks to be rejuvenated one or more times to increase their useful life substantially compared to present practice, but also increase the initial design life of disks by removing non-detectable cracks before service.

OBJECTIVES

The principal goal of this program was to demonstrate the feasibility of HIP and refinishing procedures to remove or neutralize defects which limit the fatigue life of aircraft gas turbine disks. These defects are both fabrication and service induced, and include surface connected cracks and pre-crack initiation fatigue damage.

The specific objectives of this program were to

- Develop a coating which would (1) be mechanically and chemically compatible with Ti-6Al-4V, (2) not degrade fatigue properties, and (3) bridge surface connected fatigue cracks.
- Induce controlled amounts of fatigue damage into fatigue specimens; both pre-crack initiation damage and surface cracking damage types.
- Assess the response of the different types of fatigue damage to the rejuvenation processes by comparison of total fatigue lives.
- Metallographically characterize the fatigue damage and the effect of the rejuvenation process on this damage.

PROGRAM PLAN

To meet the objectives of the program, four important areas had to be addressed, coating development, inducing controlled fatigue damage, HIP parameters, and metallographic studies. Because the rejuvenation of surface connected fatigue cracks was to be studied, the development of an appropriate coating was necessary to bridge these cracks and render them amenable to closure and bonding during HIP. To ensure the highest likelihood of success, the coating should be chemically and mechanically compatible with the substrate so as to be least likely to impair the fatigue properties of the substrate material. For these reasons a coating having the same composition as the Ti-6Al-4V fatigue specimens was sought and subsequently developed. It was realized that bridging of cracks is a difficult task, and this area has not received much attention. However, rather than emphasize bridging alone, it was believed the prudent course was to develop a compatible coating with the expectation that some bridging would occur which, in turn, would allow an assessment of both the effects on fatigue damage rejuvenation and a more specific identification of the coating problem areas.

Another important area was to induce defects, representative of those expected in gas turbine disks, into the test material. To simulate this type of damage it was desirable to induce surface-connected non-critical cracks in smooth test bars. This could be achieved if a suitable fraction of the fatigue life existed between crack initiation and failure. The point of crack initiation was to be defined in terms of some pre-selected reproducible test parameter such as: a percentage of decrease in load, an increase in specimen compliance, or an increase in mean displacement. The test parameter was to be supported by microscopic evidence of surface cracks.

The program was first intended to study mill annealed material because this is representative of the condition of most disks in service today. However, since the crack propagation period in mill-annealed material was too short, a βSTOA heat treated condition which did have an adequate crack propagation period was adopted as the material condition for this program. In addition, a procedure for sensitively monitoring the peak load during strain cycling enabled crack initiation to be detected easily during the test. This procedure was corroborated by the presence of visible surface cracks.

The HIP conditions to which the predamaged specimens were to be exposed were important to the extent that for a fixed pressure too high a combination of temperature and time would coarsen the microstructure and degrade the subsequent fatigue life. Too low a temperature and time would not cause the cracks to close and bond. The criteria used to decide the HIP conditions was to select a temperature and time in the lower range at which successful diffusion bonding of Ti-6Al-4V was previously obtained,[11,12] and to exert the maximum possible pressure.

The fatigue damage and its response to HIP were studied using metallographic techniques to gain some understanding of the underlying mechanisms of the damage and rejuvenation processes. Selected specimens in both the predamaged and in the predamaged plus treated conditions were studied.

The initial test matrix shown in Table 1 indicates the attention to the establishment of good baseline data on the effect of the different process steps and to the effect of each process step on the damaged properties. Because of considerations such as inadequate bridging of the cracks by the coating, alternative heat treatments, and program constraints, the final test matrix differed from this (Table 2): principally, several of the cracked specimens were given a second coating plus HIP treatment after it was observed in pilot studies that the cracks had not been healed by the first coat plus HIP cycle.

TABLE 1. ORIGINAL REJUVENATION TEST MATRIX

Condition	Tensile	Undamaged Fatigue	Damaged Fatigue Level 1[a]	Damaged Fatigue Level 2[b]
Base-line	X	X		
HIP	X	X	X	X
Coat and Refinish	X	X	X	X
Coat and Refinish and HIP	X	X	X	X

(a) Level 1 is pre-crack initiation damage.

(b) Level 2 includes surface-connected cracks.

TABLE 2. FINAL REJUVENATION TEST MATRIX

Condition	Undamaged Fatigue	Damaged Fatigue Level 1[a]	Damaged Fatigue Level 2[b]
Base-line	X		
HIP	X	X	
Coat and Refinish	X		
Coat and HIP	X	X	X
Coat and Overcoat and HIP			X
HIP and Overcoat and HIP			X
Coat and HIP and Overcoat and HIP			X

(a) Level 1 is pre-crack initiation damage.

(b) Level 2 includes surface-connected cracks.

EXPERIMENTAL PROCEDURE

Material

The Ti-6Al-4V alloy was obtained from Alloy Specialties, Ltd., Garden Grove, California, as one-inch diameter, centerless ground bar. The bar was fabricated from a 30-inch diameter ingot, Heat Number 12476, by Teledyne Titanium, by first press forging the ingot to 6-inch square bar followed by rolling to 1-inch diameter oversize bar. The bar was annealed at 704 C (1300 F) for 2 hours, air cooled, (mill-annealed condition) and then centerless ground to dimension. The finished 1-inch diameter bar conformed to AMS 493DA for ELI material except for aluminum and oxygen content.

The vendor-supplied report on the material included the analysis in weight percent as 6.58 Al, 4.19 V, 0.015 C, 0.16 Fe, 72 ppm H, 0.0096 N, 0.16 O, balance Ti. The β-transus was given as 963 ± 14 C (1765 ± 25 F). The results of two tensile tests conducted at Battelle showed the following average properties: modulus 17.3 x 10^3 ksi, 141.1 ksi tensile ultimate, 127.5 offset yield, 24 percent elongation in 2 diameters, 44.4 percent area reduction and a true fracture stress of 187.8 ksi. These properties correspond closely to those reported by the vendor* and exceed typical handbook values.[4]

During a preliminary investigation, it became apparent that the material in a mill-annealed condition could not be used to meet the objectives of the program, but a βSTOA heat treatment rendered it usable. The βSTOA treatment consisted of a solution treatment of 1010 C (1850 F), 1.5 hr, water quench, followed by aging at 732 C (1350 F), 3 hr, air cool. The resulting microstructure was tempered martensite as shown in Figure 1. The prior β grain size evident in Figure 1a was relatively large because of the beta solution treatment. All the fatigue specimens possessed a duplex grain size. As shown in Figure 2 a finer grained core (ASTM M-13.5 grain size) extending the length of the specimen was contained within a coarser grained sheath (ASTM M-12 grain size).

Tensile properties for the material in this condition were: modulus 16.45 x 10^3 ksi, 153.4 ksi tensile ultimate, 144.0 ksi offset yield, 8.35 percent elongation in 2 diameters, 10.8 percent area reduction and a true fracture stress of 169.2 ksi.

---

* Tensile properties in the mill-annealed condition were quoted as 143.2 ksi tensile ultimate, 132.6 ksi yield strength, 15.3 percent elongation in 4 diameters, 44.2 percent area reduction and hardness of 31 R_C.

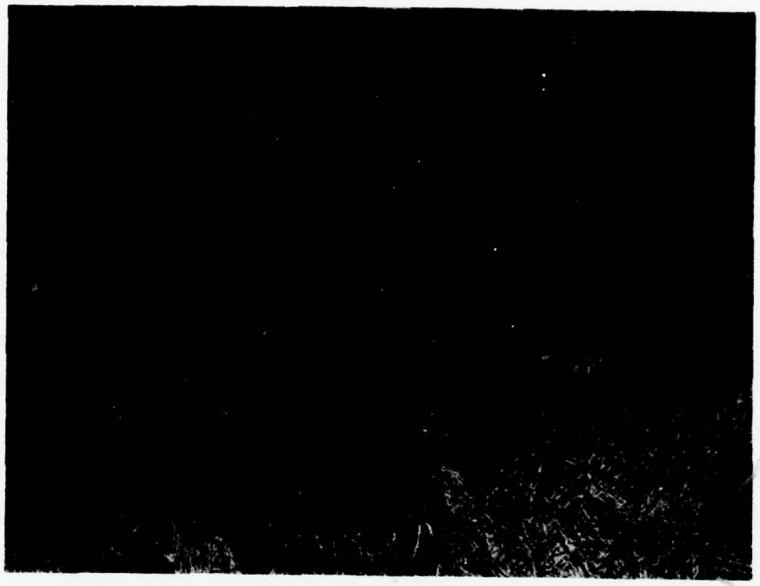

a. 50 X

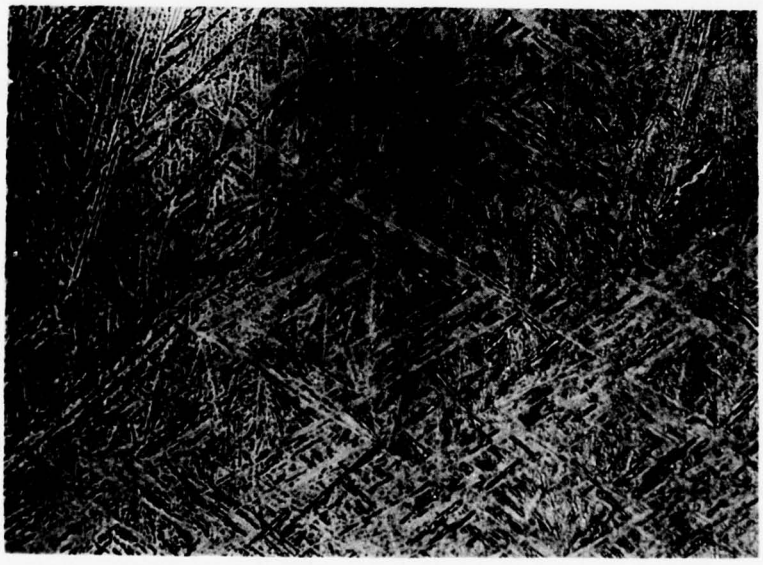

b. 500 X

FIGURE 1. MICROSTRUCTURE OF Ti-6Al-4V IN THE βSTOA CONDITION USED FOR THE FATIGUE EXPERIMENTS

FIGURE 2. THE DUPLEX GRAIN STRUCTURE IN THE FATIGUE SPECIMENS, MADE UP OF A FINE-GRAINED CORE IN A COARSEN-GRAINED SHEATH

Fatigue Testing

Specimen

All specimens used in this investigation were of the geometry shown in Figure 3. Note that this geometry provides a reduced section 0.75 inch in length and 0.375 inch in diameter. This rather stocky geometry was chosen in an attempt to provide a reasonable section for crack propagation, a large surface free from extensometer knife edges to permit surface replication for damage studies and a reasonably high buckling load for testing in a low to moderate capacity test system. A total of 75 specimens were fabricated; the machining being performed at Met-Cut, Cincinnati, following their low-stress cylindrical grind procedure detailed in Table 3.

The first 50 specimens were machined from mill-annealed material and then given the βSTOA heat treatment. These specimens were numbered from 1 to 50. The remaining 25 specimens were machined from 5-1/8-inch long, 1-inch diameter blanks after βSTOA heat treatment.* These specimens were numbered 1A to 25A. Of these 75 specimens, 2 were used as setup and procedure verification samples and 3 were damaged during setup on the initial loading, and therefore not used. The deposition of the remaining samples was as follows: 3 to 13 and 16 were committed to the initial study of the material in the mill-annealed condition, the results of which have been reported in Appendix A; 40 to 50 were committed to the exploratory heat treatment study as detailed in Appendix B; while the remainder were committed to the study of HIP rejuvenation of fatigue damage on the βSTOA material.

Apparatus and Procedure

Each of the experiments in this program was performed in one of three similar servocontrolled electrohydraulic test systems. All testing was performed in strain control. Specimens were subjected to a fully reversed, sinusoidal pacing function. The environment was ambient laboratory air, nominally 21 C (70 F) and 40 percent humidity.

Strain was controlled over a 0.750-inch gage length using a clip-on extensometer calibrated to ASTM Class B_1. Strain was programmed to follow a sinusoidal waveform at frequencies ranging from 0.1 Hz to 30 Hz, depending on the amplitude of the control strain. The ability of the extensometer to operate over this range of frequencies was independently verified as a function of the strain amplitude prior to beginning the test program. To ensure the temperature of the reduced section remained ambient in tests with either large strain amplitudes or higher frequencies, the frequency was chosen so that the indicated temperature (monitored via a

* The microstructure of the specimens were the same for both lots as seen by optical metallography (Figure 1).

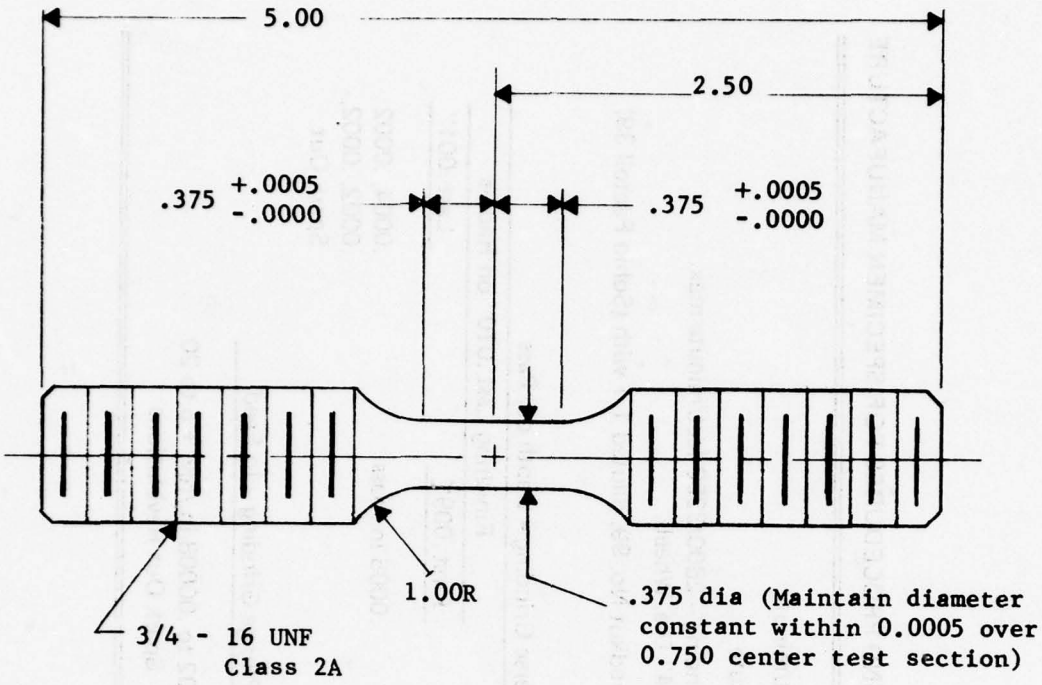

FIGURE 3. GEOMETRY OF THE FATIGUE SPECIMEN

TABLE 3. CYLINDRICAL GRIND PROCEDURES FOR SPECIMEN MANUFACTURE

Work Surface: 8 to 26 feet/minute

Table Speed: 7 inches/minute

Wheel Speed: Traverse Grinding - 2800/3250 feet/minute max.
(12" to 14" Dia. Wheel)

Grinding Fluid: Stuart Thredkut No. 99, diluted 1.1 with (Sohio Factoil 39)

Traverse Grinding - Depth per Pass		
	Finishing Last .010" on Radius	
Roughing	First .009"	Last .001"
.001 in./pass	.0005 in./pass	.0004, .0002 .0002, .0002, Spark Out

Plunge Grinding - In Feed
.00002 to .00008 in./rev. + 5 to 20 Spark Out Revolutions

thermocouple looped about and in contact with the test section) remained constant within 2.8 C (5 F) during testing. Strain was controlled to within 1 percent of the programmed signal. The extensometer calibration was performed and verified several times during the test program.

Load was monitored in all tests using a commercially available load cell mounted in series with the specimen. Calibration of the load cell was performed prior to and verified once during the test program. The load cell was observed accurate and linear within 0.1 percent of the operating range used in the present program. A peak load detector was incorporated in the control loop for use in determining crack initiation based on load drop from the saturation (stable cyclic) load (stress) level.

All specimens were gripped in a fixture arrangement similar to that detailed in Reference 5. It is noteworthy that such an arrangement features a liquid-solid Woods metal grip which serves to minimize specimen mounting stresses. Prior to commencing the test program, the alinement was adjusted to minimize bending strains; the adopted standard being bending strains less than 1 percent of the imposed axial strain.

Monotonic and cyclic deformation response was recorded continuously during the first ten cycles and at logarithmic intervals thereafter on an X-Y recorder; while both load and strain were continuously recorded on a time-based, high-speed strip chart recorder.

Before commencing with the experimental program, the closed loop system was tuned to allow testing at the optimum system gain. Concurrently, the load cell and extensometer were calibrated along with the related recording devices. After this preliminary phase, the test phase began. The procedure used for each test follows: after mounting the specimens in the upper grip, the load train was closed and load control and the liquid-solid grip frozen. Maintaining the system at zero load, the extensometer was mounted and zero suppressed and all recording devices activated and zero suppressed. The system was then shut down and strain control selected. The system was then reenergized and allowed to stabilize before strain cycling. In tests where the system had to be periodically shut down and restarted (such as for surface damage replication, Appendix B) care was taken to unload and thereafter reload without inducing spurious mean stresses. All tests were terminated as required either to induce a prescribed level of damage or to generate some baseline life to initiation and fracture data.

Test Program

Table 4 details the final test program to generate results useful in assessing the feasibility of HIP rejuvenation of fatigue damage in βSTOA Ti-6Al-4V. This matrix was evolved with consideration given to the results of preliminary testing of the material, first in the mill-annealed condition (Appendix A), thereafter in various heat treatments culminating in the choice

TABLE 4. FATIGUE REJUVENATION PROGRAM TEST MATRIX

Material Condition	Undamaged	Fatigue Damaged Level 1	Fatigue Damaged Level 2
As heat treated[a]	2, 18, 21, 24, 25, 26, 30, 33, 38, 39 1A, 2A, 3A, 5A, 6A, 7A, 8A, 9A, 10A, 11A		
As heat treated[b]	14A		
	Single HIP		
HIP[b]	14, 22A, 23A	21A, 28	
Coated[b]	22		
Coated + HIP[b]	29, 36, 37	15, 17A, 18A, 25A, 34	1
Coated + overcoat + HIP[b]			12A, 13A
	Double HIP		
HIP + overcoat + HIP[b]			27, 20A, 31
Coated + HIP + overcoat + HIP[b]	19A, 32		15A, 16A

(a) Tested at total strain ranges from 0.9 to 4.0 percent.
(b) Tested at a nominally identical total strain range of 1.50 percent.

Coated: A permanent 3 to 4 mil-thick coating of nominal Ti-6Al-4V.

Overcoat: Sacrificial coating of electrodeposited nickel.

- 'A' designation were heat treated as bar stock, then machined; the other specimens were machined, then heat treated.
- All coated specimens were peened with glass beads after coating.
- All specimens were polished longitudinally before fatigue testing.

of the βSTOA condition (Appendix B). Subsequently, further tests were performed to establish the strain amplitude for the ensuing feasibility assessment. That strain amplitude had to concurrently satisfy three requirements: (1) be sufficiently inelastic so as to reduce fatigue scatter, (2) be sufficiently small so as to induce fatigue fracture at levels greater than 10^3 cycles and (3) give rise to a reasonable fraction of life spent in propagating a fatigue crack from observable surface damage. That strain level was determined from the results of 20 tests which encompassed strain ranges from 4 percent to 0.90 percent to be 1.50 percent, the results being presented in Table 5.

To differentiate between the different levels of fatigue damage the specimens were subjected to prior to the rejuvenation treatments, the following designations are introduced.

- Level Zero pre-damage represent specimens given no previous fatigue cycling.
- Level One pre-damage represents specimens cycled just short of crack initiation.
- Level Two pre-damage represents specimens having one or more visible surface cracks at 30 X.

Coating Procedures

Ti-6Al-4V Coating

A 24-inch stainless steel water-cooled vacuum chamber was tooled for these electron-beam vacuum deposition experiments. The chamber was pumped by a 6-inch, freon-trapped, high-speed oil diffusion pump. The base pressure of the system was 8×10^7 torr. The electron-beam gun evaporation source was a 14,000-watt, 270-degree bent beam commercial model. The source material was fed into the bottom of the hearth of the electron-beam gun from a 1-1/2-inch-diameter ingot. An existing 5500-watt quartz lamp furnace was modified for these experiments. This modification included removal of all insulation and other possible sources of contamination due to the extremely reactive nature of titanium vapor. The furnace would heat and continuously rotate seven bars at a distance of 10 inches above the source, or heat about 20 square inches of flat coupon surface.

Nickel Electroplate

Late in the program, nine test bars were electroplated with a sacrificial nickel coating over the reduced section in an attempt to bridge cracks not bridged by the titanium alloy coating. Nickel was selected because it is simple and economical to apply a sound coating, and it could be removed chemically, eliminating a machining step. Because of the difficulty in regenerating a true

TABLE 5. RESULTS OF THE PRELIMINARY STUDY OF THE FATIGUE RESISTANCE OF βSTOA Ti-6Al-4V

Specimen Number	Strain Range, percent			Cycles			Comments on Failure
	Control Δe^t	Stable Δe^e	Components Δe^p	To Initiation	To Fracture	N_i/N_f%	
2	2.57	1.63	0.94	58	86	–	Invalid - broke outside gage length
18	3.06	1.58	1.48	74	139	53.2	Valid
21	2.03	1.54	0.49	215	241	89.2	Valid
24	0.92	0.92	–	195,059[a]	–	–	–
25	1.00	1.00	–	122,129[a]	–	–	–
26	2.58	1.68	0.90	85	105	81.0	Valid
30	2.04	1.51	0.53	298	354	84.2	ditto
33	4.06	1.80	2.26	23[b]	–	–	"
38	1.40	1.34	0.06	5,120	5,142	99.6	"
39	1.40	1.37	0.03	3,993	4,553	87.7	"
1A	2.01	1.50	0.51	933	1,029	90.7	"
2A	1.00	0.989	0.011	165,953	167,148	99.3	"
3A	1.00	1.00	–	600,000[a]	–	–	–
5A	1.24	1.235	0.005	4,305	4,785	90.0	Valid
6A	1.17	1.155	0.015	16,180	18,097	89.0	ditto
7A	1.10	1.09	0.01	42,300	43,300	97.7	"
8A	1.10	1.10	–	23,050	24,475	94.0	"
9A	1.08	1.08	–	645,000[a]	–	–	–
10A	3.00	1.64	1.36	70	121	57.9	Valid
11A	2.57	1.54	1.03	220	243	90.5	Valid

(a) Test suspended before initiation.
(b) Test suspended before failure; used for metallography.

surface on the threaded grip ends, an elastomeric stop-off compound was used to prevent plating on the threads. A double plating procedure with an intervening shot blast treatment produced a high-quality nickel plate 0.010 inch-thick based on visual inspection. A build-up of nickel at the edge of the plated area was removed by machining to ensure removal of any overlapped elastomer. Organic material decomposing during the HIP cycle is very damaging to the HIP equipment and possibly to the specimens.

After HIP, the nickel plating was removed by pickling in a 2% nitric acid solution at 65 C (149 F). After pickling, the test bars were vacuum heat treated at 760 C (1400 F) to remove any hydrogen from the electroplating or pickling steps. Then, the test bars were abraded and tested according to the procedure previously reported.

Visual examination of the test specimens indicated that the nickel plating was not completely adherent. The reaction layer normally associated with a nickel-titanium diffusion couple after exposure to the high temperature of the HIP cycle only partially covered the specimen surfaces, indicating that the nickel plate and Ti-6Al-4V substrate were not in intimate contact over much of the specimen surface before HIP.

HIP Procedures

First HIP Cycle

After coating with the Ti-Al-V coating, the predamaged and control specimens were lightly peened with clean glass shot to introduce some work into the PVD coating and promote bonding during HIP. A driving air pressure of 20 psi was used to impel the glass shot against the specimens while rotating them at 4 rpm. Peening of each specimen was continued for only 30 seconds to avoid the formation of a stress gradient sufficient to separate the coating and substrate. (An initial peening trial at 35 psi driving pressure did result in buckling of the coating in the shoulder transition section of a slightly oxidized specimen.) The specimens were then blown clean with air, visually examined, and HIP without further preparation.

A total of twenty mechanical test specimens, identified in Table 6, were suspended from cables as shown schematically in Figure 4 and HIP in a single autoclave cycle. This method of specimen support was used to prevent any chance of buckling or binding of the specimens during HIP as even the slightest deformation would have rendered them useless for further axial fatigue testing. This initial HIP experiment was conducted at 843 C (1550 F) and 23,000 psi argon for 3 hours as summarized in Figure 5. Autoclave pressure was maintained below 1000 psi during the initial heating portion of the HIP cycle to promote the ductility of the PVD coatings prior to increasing the pressure to its maximum attainable level. After the specimen temperature

TABLE 6. SPECIMENS PROCESSED IN FIRST HIP CYCLE

Specimen No.	Predamage Level	PVD Coating Cycle No.
1	2	1
14	0	Uncoated
15	1	2
17	1	Uncoated
27	2	Uncoated
28	1	Uncoated
29	0	1
31	2	Uncoated
32	0	1
36	0	2
37	0	2
15A	2	1
16A	2	1
17A	1	2
18A	1	2
19A	0	1
20A	2	Uncoated
21A	1	Uncoated
22A	0	Uncoated
23A	0	Uncoated

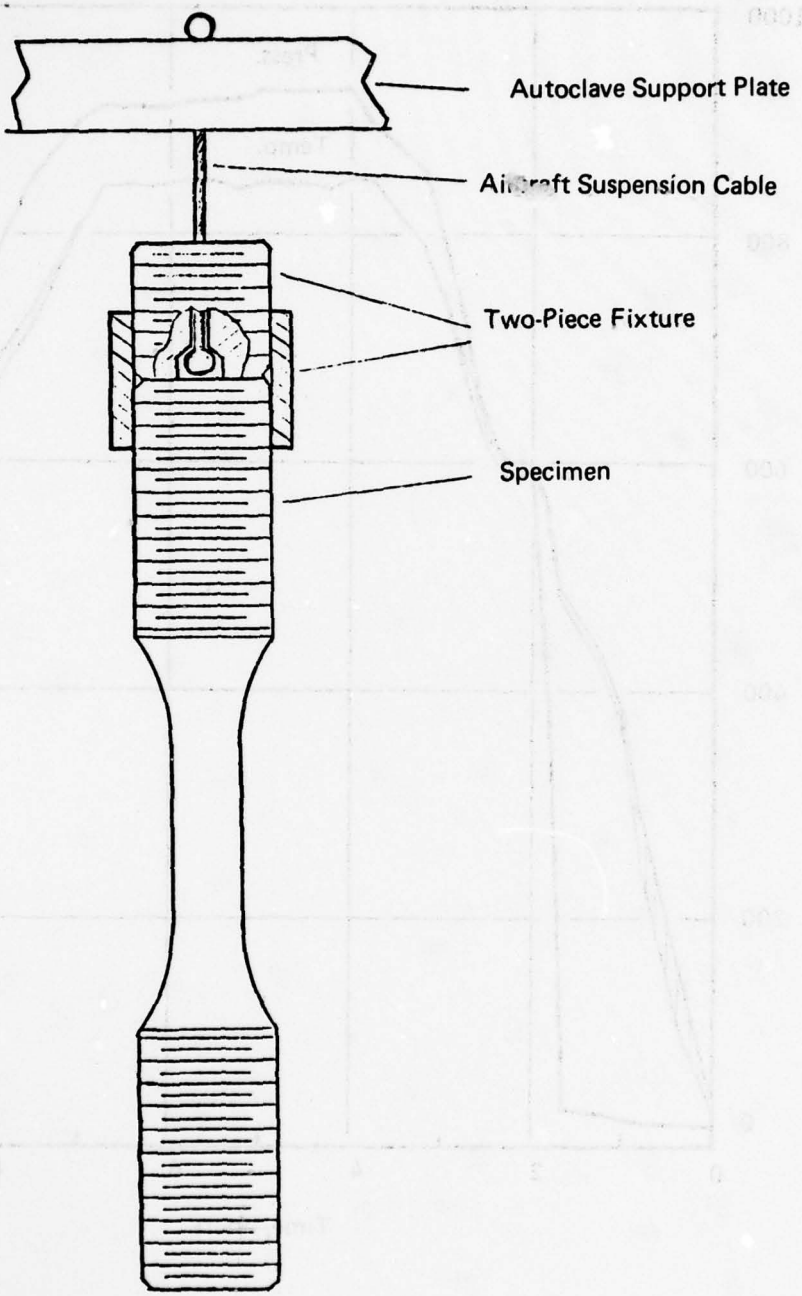

FIGURE 4. TEST SPECIMEN HIP SUPPORT ASSEMBLY

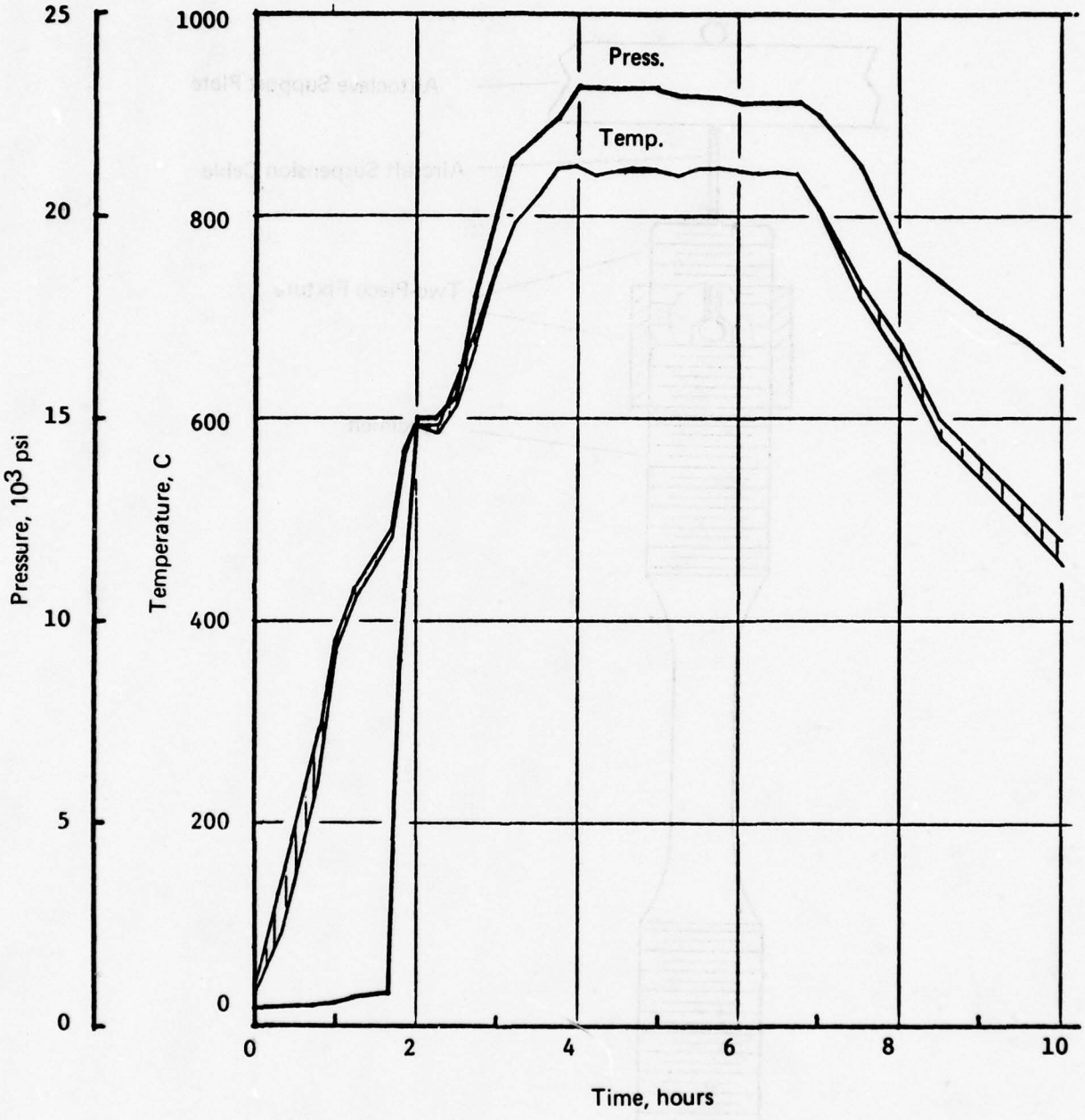

FIGURE 5. TEMPERATURE AND PRESSURE HISTORY OF FIRST REJUVENATION HIP CYCLE

had reached 480 C (864 F), pressurization of the autoclave was resumed until the maximum available level (15,000 psi) was attained without the use of mechanical booster compressors. Use of these compressors could cause excessive contamination of the HIP atmosphere. Pressure was then allowed to increase by thermal expansion to maximum pressure of 23,000 psi during the remainder of the heating period. During the three hour steady state portion of the HIP cycle the temperature varied less than 5 C (9 F) as indicated by three thermocouples placed among the specimens. After the prescirbed 3 hours at temperature and pressure, the autoclave heater was turned off and the specimens allowed to cool under pressure. Upon their removal from the HIP vessel, the specimen surfaces were found to be lightly oxidized.

Second HIP Cycle

A total of ten mechanical test specimens identified in Table 7 were given a second HIP after nickel electroplating. Titanium chips were placed adjacent to the specimens to reduce surface oxidation resulting from impurities in the HIP gas. This experiment paralleled the first except that the heat-up and pressurize cycle was altered and a higher ultimate pressure, 28,000 psi, was attained as shown in Figure 6. To maintain intimate contact between the nickel and titanium, despite the unfavorable thermal expansion characteristics of nickel relative to titanium, the autoclave was pressurized to 3000 psi at room temperature and cryogenically pumped to 15,000 psi during the initial heat-up portion of the HIP cycle.

Metallography

The metallographic specimens were prepared using standard grinding and polishing techniques. The etchant used was 95% H_2O, 3.5% HNO_3, and 1.5% HF in volume percent.

TABLE 7. SPECIMENS PROCESSED IN SECOND HIP CYCLE

Specimen No.	Predamage Level	Previous HIP	Coating Type
(a)			
22	0	No	None
27	2	Yes	Electroplate
31	2	Yes	Electroplate
32	0	Yes	PVD + electroplate
12A	2	No	PVD + electroplate
13A	2	No	PVD + electroplate
15A	2	Yes	PVD + electroplate
16A	2	Yes	PVD + electroplate
19A	0	Yes	PVD + electroplate
20A	2	Yes	Electroplate

(a) Dummy specimen.

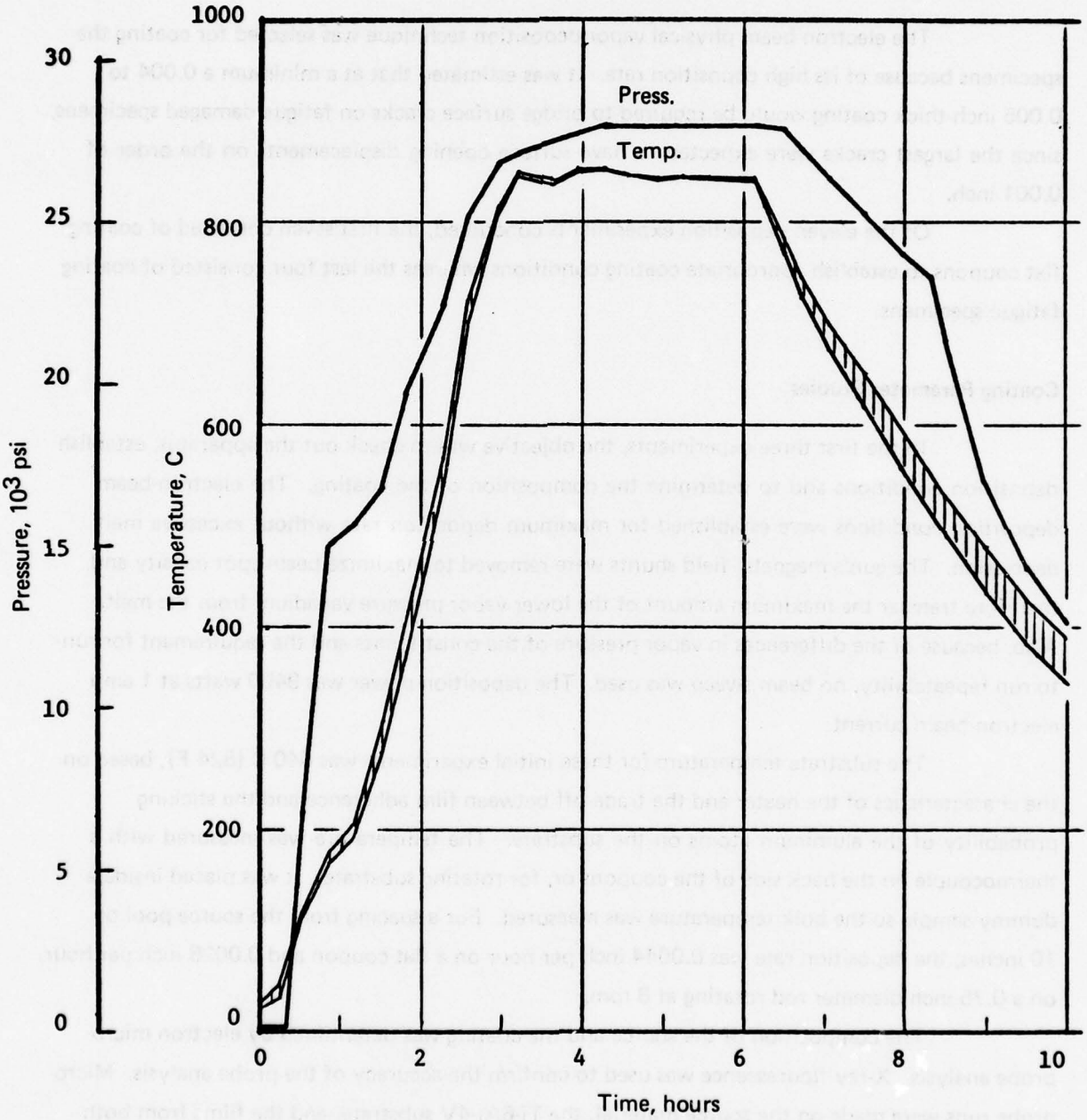

FIGURE 6. TEMPERATURE AND PRESSURE HISTORY OF SECOND REJUVENATION HIP CYCLE

RESULTS

Coating Studies

The electron beam physical vapor deposition technique was selected for coating the specimens because of its high deposition rate. It was estimated that at a minimum a 0.004 to 0.005 inch-thick coating would be required to bridge surface cracks on fatigue damaged specimens, since the largest cracks were expected to have surface opening displacements on the order of 0.001 inch.

Of the eleven deposition experiments conducted, the first seven consisted of coating flat coupons to establish appropriate coating conditions whereas the last four consisted of coating fatigue specimens.

Coating Parameter Studies

In the first three experiments, the objective was to check out the apparatus, establish deposition conditions and to determine the composition of the coating. The electron-beam deposition conditions were established for maximum deposition rate without excessive melt depression. The gun's magnetic field shunts were removed to maximize beam spot density and therefore transfer the maximum amount of the lower vapor pressure vanadium from the melt. Also, because of the differences in vapor pressure of the constituents and the requirement for run-to-run repeatability, no beam sweep was used. The deposition power was 9400 watts at 1 amp electron-beam current.

The substrate temperature for these initial experiments was 440 C (824 F), based on the characteristics of the heater and the trade-off between film adherence and the sticking probability of the aluminum atoms on the substrate. The temperature was measured with a thermocouple on the back side of the coupons or, for rotating substrates, it was placed inside a dummy sample so the bulk temperature was measured. For a spacing from the source pool of 10 inches, the deposition rate was 0.0044 inch per hour on a flat coupon and 0.0028 inch per hour on a 0.75-inch diameter rod rotating at 8 rpm.

The composition of the source and the coating was determined by electron micro-probe analysis. X-ray flourescence was used to confirm the accuracy of the probe analysis. Micro-probe runs were made on the source material, the Ti-6Al-4V substrate, and the films from both deposition runs, and the best value of avarage coating composition determined. About 27 percent vanadium loss and 25 percent aluminum loss occurred from the initial source composition to the

coating composition. This loss was due to the differences in the vapor pressures, scattering properties, and sticking coefficients of the constituents.

As a result of the analysis of the coatings deposited in the first runs, a source ingot of the required modified composition was prepared from at Ti-6-4 rod with added aluminum and vanadium. This ingot was then quartered, the quarters inverted and welded together. This ingot was again vacuum arc melted to insure homogeneity of the constituents. The overall composition (weight percent) of the final electron beam source ingot was Ti-7.04Al-4.74V, within acceptable limits of the Ti-7.5Al-5.1V requested.

Four runs were then made to evaluate the composition of the coatings prepared from the ingot of modified composition and determine whatever modifications were necessary in the deposition process to deposit films of composition as nearly as possible to Ti-6.0Al-4.0V. Forty-five, one inch diameter Ti-6Al-4V disks were coated for evaluation.

Initially, two coupons were coated in the same run on one side only to a thickness of about 0.010 inch using the Ti-7.04Al-4.74V ingot as source material. Electron probe micro-analysis of the deposited film indicated a uniform concentration of vanadium at about 4.1 percent but a wide variation in aluminum content from 3.4 to 9.4 percent. To determine whether this variation was caused by inhomogeneity in the source ingot a second run was made.

Electron microprobe traces across the thickness of the coated specimens showed a pattern of variation in aluminum content which was consistent between specimens coating in a single experiment and in separate coating experiments. As shown in Figure 7 the aluminum content of the coated specimens rose sharply at the coating-substrate interface and then fell rapidly to approximately half the substrate aluminum content through the remainder of the coating thickness. The consistency of this pattern eliminated source ingot inhomogeneity as the reason for variation in the coating composition.

Review of the coating experiment histories revealed that substrate temperature increased rapidly by some 30 C (54 F) upon exposure to the molten surface of the source ingot. This increase in temperature from 450 to 480 C (842 to 896 F , which is caused by direct radiation from the source ingot and the heat of condensation given up by the depositing coating, did not seem particularly excessive. However, the rate of change of the substrate temperature with time correlated very well with the observed fluctuation in aluminum content of the coatings. This suggested that the rate of deposition or retention of aluminum in the deposited film is extremely sensitive to substrate temperature. This hypothesis was verified by a third coating experiment in which the substrate temperature was held relatively constant at about 400 C (752 F). Electron microprobe analysis of one specimen from this experiment showed that, except for a brief decrease at the coating-substrate interface, the aluminum content of the coating was significantly higher than that of the substrate.

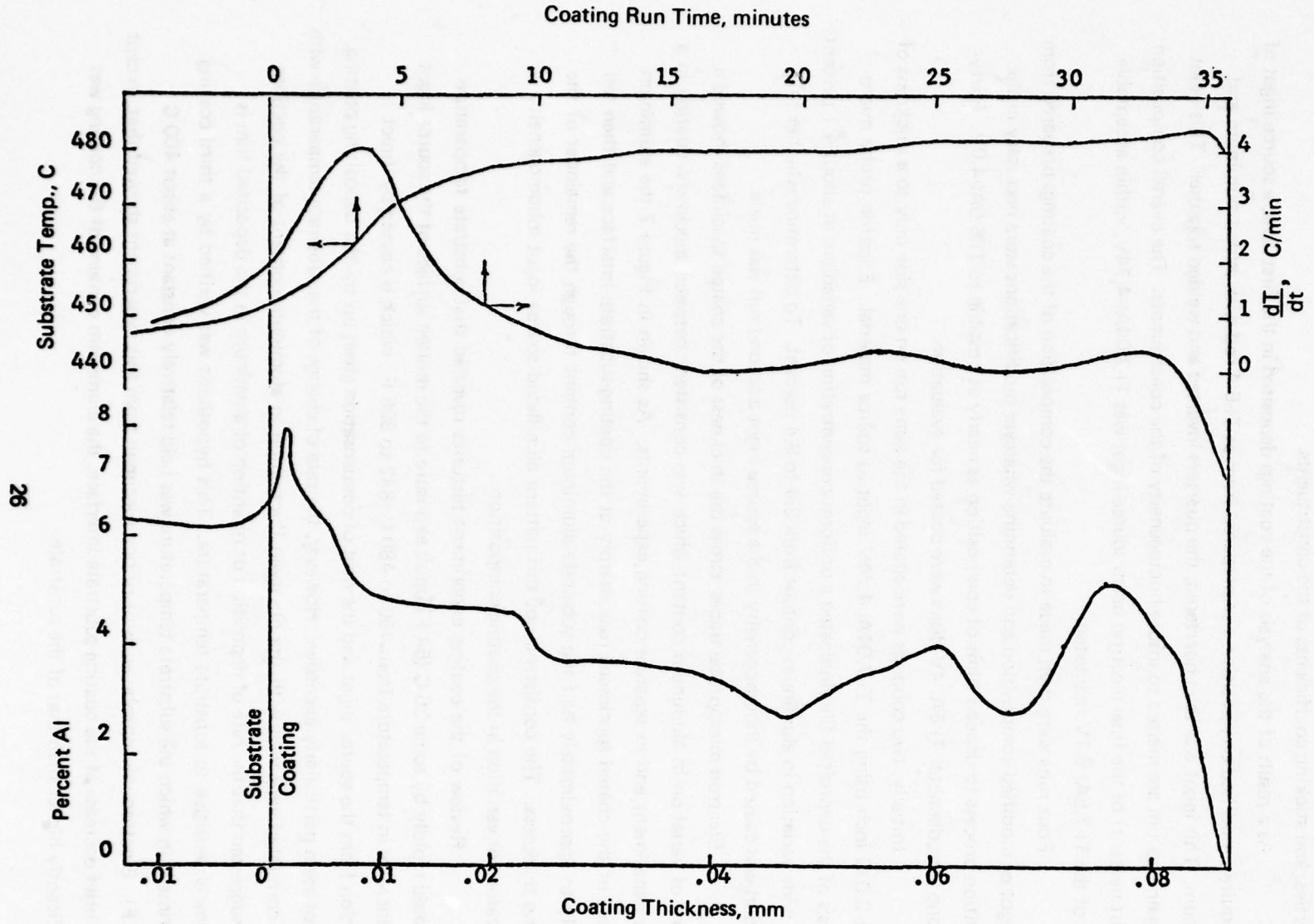

FIGURE 7. COMPARISON OF SMOOTHED MICROPROBE PROFILE FOR ALUMINUM WITH SUBSTRATE TEMPERATURE COATING

The effects of reducing substrate temperature during coated deposition were not entirely beneficial, however, as a marked decrease in the adherence of the deposited film was noted. Both the aluminum content and adherence of Ti-Al-V coatings on Ti-6Al-4V are extremely sensitive to temperature and temperature changes in the substrate. Subsequently, modifications in the substrate heater, the thermocouples, and the deposition procedure were made which permitted holding the substrate temperature uniform at 450 to 453 C (842 to 848 F) throughout the runs. Both the adherence and composition of aluminum were then acceptable.

A new source ingot having a composition Ti-7.50Al-4.92V was prepared for coating the fatigue specimens. In checking out the heating-rotating fixture it was determined that adequate thickness uniformity could be achieved over seven rotating specimens at a deposition rate of 0.004 inch per hour. The specimens were rotated at 8 rpm.

Seven fatigue test specimens were coated with approximately 0.004 inch of Ti-6Al-4V in one run. Six fatigue specimens plus a metallographic specimen were coated in the next run, and five fatigue specimens and a metallographic sample were coated in the last run. The critical parameter of substrate temperature was maintained at 453 C (848 F) during all depositions. As expected, this low substrate temperature resulted in marginal adherence but was necessary to insure that the required aluminum composition was deposited. The films were deposited at pressures as low as 1.5×10^{-6} torr so that the films were bright and the columnar structure was dense. The depositions went as expected with two exceptions. The Ti-7.5Al-4.9V source ingot was slightly porous so that there was some spatter during the depositions. Also the rotation chain fell off of one side of the furnace during the last run resulting in three specimens being coated unevenly (one of which was the metallographic specimen).

Microstructure

The objective of the coatings, to completely bridge over surface cracks, was only partially realized as discussed in detail later. Examples of the character of the coating over fatigue-induced cracks are shown in Figure 8. In Figure 8a a narrow crack less than 0.001 inch wide at the surface appears as bridged over, although there are coating defects which appear as folds or heavy lines above the crack which might allow the pressurized gas to enter the crack during HIP. For cracks having wider openings, as in Figure 8b, the coating was unable to bridge the crack, and no closure would occur during subsequent HIP. Further evidence of the failure of the coating to close a possible fatigue crack is shown in Figure 9. This is an as-coated surface.

The coatings have a columnar structure as expected, but also show some layering caused in part by the discontinuous build-up of the coating by rotating the specimens.

The influence of various thermal and mechanical treatments on the coatings are described in Appendix D.

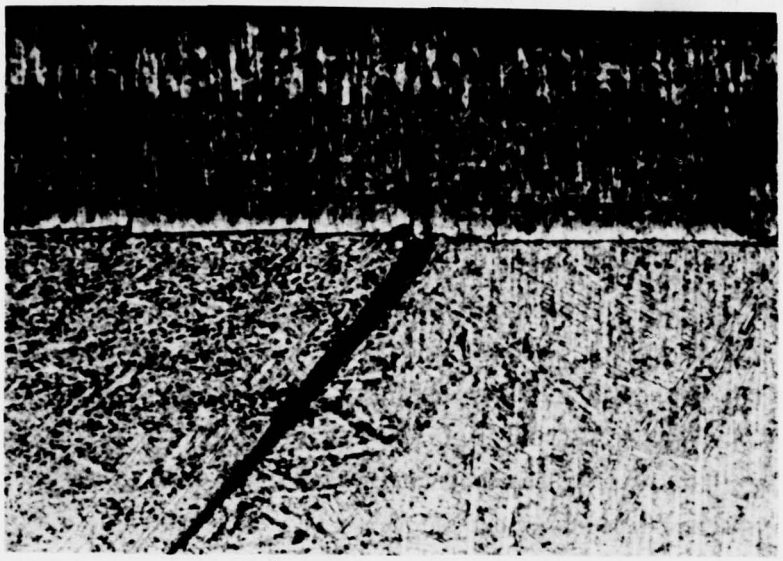

a.

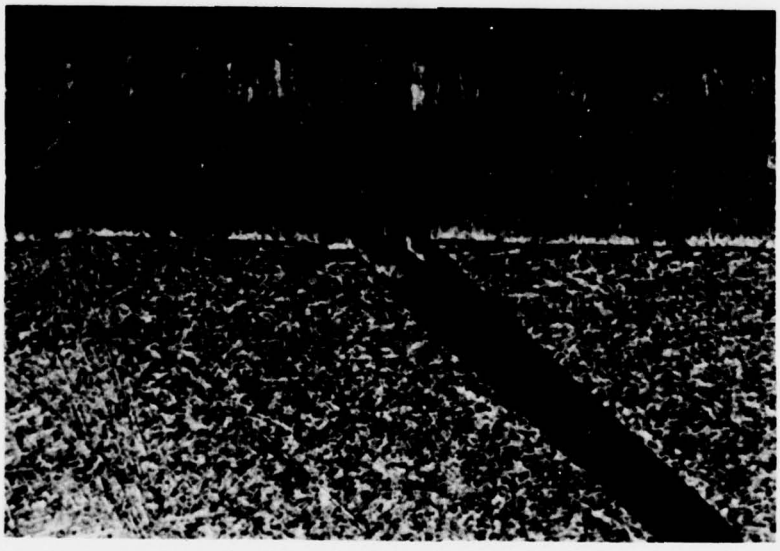

b.

FIGURE 8. APPEARANCE OF COATING OVER SURFACE FATIGUE CRACKS BEFORE HIP–250X

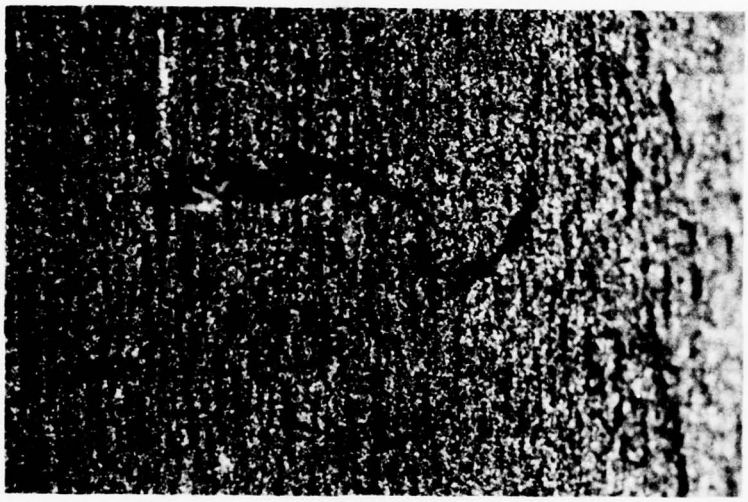

FIGURE 9. AS-COATED SURFACE SHOWING THE APPEARANCE OF THE COATING OVER WHAT IS PROBABLY A PREEXISTING FATIGUE CRACK ON THE ORIGINAL SURFACE–180X

Fatigue Studies

Results from baseline property tests on βSTOA material are tabulated in Table 5. The results in Table 5 which pertain to the relative fractions of life spent initiating and propagating cracks in the βSTOA material are plotted in Figure 10a as a function of the corresponding plastic strain range. Note from this figure that the data follow a bilinear trend. Above a plastic strain range of 0.80 percent, the relationship between plastic strain Δe^p, and the ratio N_i/N_f is given by $\Delta e^p = 4 \exp(-0.019\ N_i/N_f)$. At values of plastic strain range less than 0.80 percent, the value of the ratio N_i/N_f is 0.86 and is apparently insensitive to Δe^p over the range of Δe^p considered in this program. Also, the results for Level Zero damage specimens tested after the various treatments (tabulated in Table 8) scatter around this trend curve as shown in Figure 10b.

Since N_i/N_f is large, it is difficult to establish whether N_p (the number of cycles in the crack propagation period = N_f-N_i) or the ratio N_p/N_f remains constant; especially in view of the scatter in N_p. For these data (Specimen Nos. 14, 22A, 23A, 29, 37, 1, 32, 19A), the average propagation periods are: 369 cycles for H_1, 315 cycles for $C_T + H_1$ and 461 for $C_T + H_1 + C_N + H_2$. The overall average propagation period is 371 cycles. For the extremes in life to failure, 1452 and 3286 cycles, respectively, the extremes in the ratio N_i/N_f are 0.74 and 0.89, respectively, for the average propagation period of 371 cycles. These extremes tend to bound the corresponding observed values. This indicates that, on the average, the propagation period is constant and the rejuvenation process steps did not significantly change the material's relative ability to support a crack as compared to the βSTOA condition.

Results reported in Table 5 can also be used to characterize the fatigue resistance of the βSTOA material in the low cycle regime. Figure 11 presents the fatigue resistance on coordinates of total strain and cycles for both crack initiation and separation (fracture). Cycles to crack initiation is here defined as that life at which the tensile component of the cyclic stress response first began decreasing as compared to the stable compression response. Such a definition obviously includes a portion of the life spent propagating the fatigue crack. The curve shown for total life (life to separation) represents the sum of the life spent in crack initiation and propagation. The initiation trend line has been obtained by subtracting the number of cycles spent in crack propagation (computed using the trend curve of Figure 10a) from the total life. This line corresponds closely with the initiation data. Note that use is made here of the experimentally observed propagation period based on the above noted definition of initiation.

The crack propagation period can also be estimated using linear elastic fracture mechanics and available data[6] for material in the STOA condition. The calculated estimate of

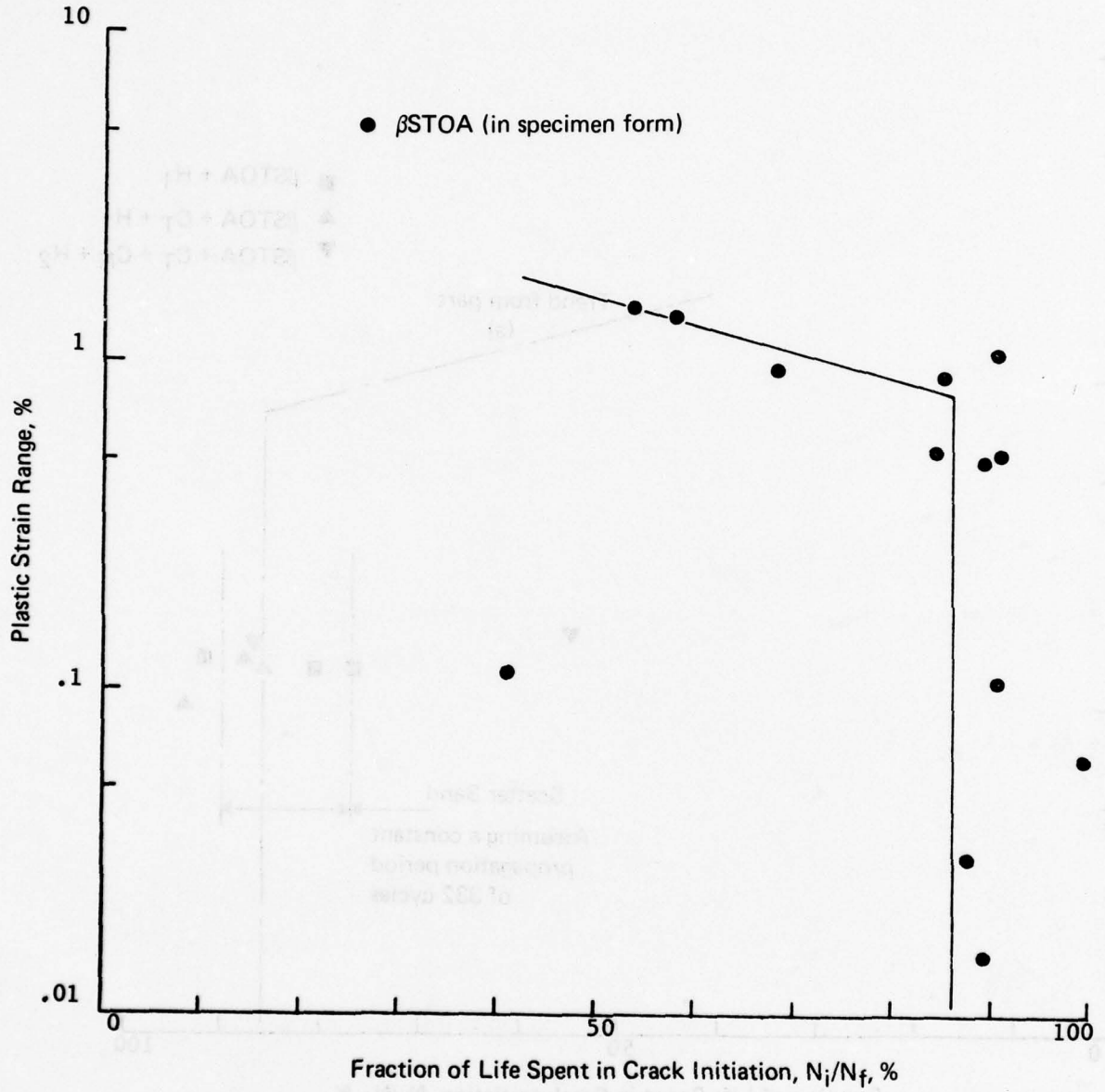

a. Baseline properties

FIGURE 10. RESULTS OF BASELINE PROPERTIES AND LEVEL ZERO PROPERTIES AFTER VARIOUS PROCESS STEPS

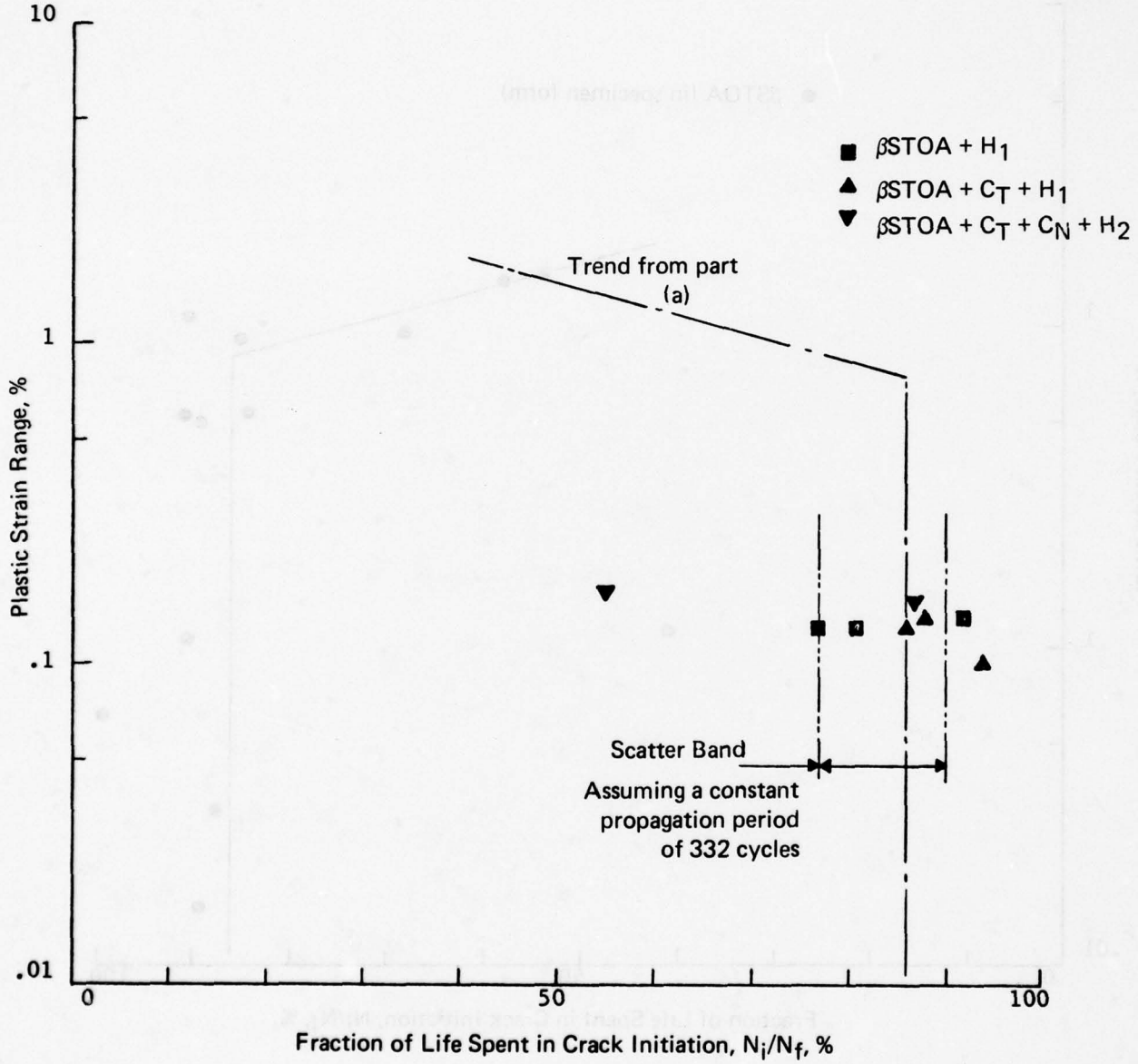

b. Level zero properties compared to baseline properties

FIGURE 10. RESULTS OF BASELINE PROPERTIES AND LEVEL ZERO PROPERTIES AFTER VARIOUS PROCESS STEPS

TABLE 8. RESULTS OF THE EXPERIMENTAL PROGRAM TO ASSESS FEASIBILITY OF HIP REJUVENATION OF FATIGUE DAMAGE - (All tests at nominally the same strain range)

Damage Level	Condition[a]	Specimen Number	Strain Range, percent: Control Δe^t	Stable Δe^p	Components Δe^e	Cycles: Of Prior Damage	To Initiation	To Fracture	Comments on Failure
0	βSTOA	14A	1.52	0.11	1.41	–	753	1851	Valid
	H_1	14	1.53	0.14	1.39	–	1339	1461	ditto
	H_1	22A	1.52	0.13	1.39	–	2260	3286	"
	H_1	23A	1.52	0.13	1.39	–	1170	1528	"
	C_T	22[b]	1.51	–	–	–	–	–	–
	C_T+H_1	29	1.52	0.14	1.38	–	2730	3102	Valid
	C_T+H_1	36	1.52	0.10	1.42	–	528	563	Invalid - broke outside gage length
	C_T+H_1	37	1.53	0.13	1.40	–	1244	1452	Valid
	$C_T+H_1+C_N+H_2$	32	1.51	0.17	1.34	–	848	1537	Valid
		19A	1.51	0.16	1.35	–	1520	1754	Valid
1	H_1	21A	1.52	0.13	1.39	750	–	2095	Valid
	H_1	17	1.53	0.12	1.41	750	–	1341	Invalid - broke outside gage length
	H_1	28	1.53	0.13	1.40	700	–	1557	Valid
	C_T+H_1	15	1.53	0.14	1.39	700	–	1919	Valid
	ditto	34[c]	1.50	–	–	693	–	–	–
	"	17A	1.52	0.10	1.42	700	–	2319	Valid
	"	18A	1.52	0.12	1.40	700	–	1275	Invalid - broke outside gage length
	"	25A[c]	1.50	–	–	65-	–	–	–
2	C_T+H_1	1	1.53	0.12	1.41	1385	–	1750	Valid
	$C_T+C_N+H_1$	12A	1.51	0.12	1.39	1102	–	1267	ditto
	$C_T+C_N+H_1$	13A	1.52	0.16	1.36	800	–	1907	"
	$H_1+C_N+H_2$	27	1.51	0.10	1.41	1100	–	1307	"
	$H_1+C_N+H_2$	31	1.51	0.12	1.39	1000	–	1589	"
	$H_1+C_N+H_2$	20A	1.51	0.14	1.37	625	–	1754	"
	$C_T+H_1+C_N+H_2$	15A	1.51	0.18	1.33	750	–	1590	"
		16A	1.51	0.16	1.35	750	–	2111	"

(a) C_T = Coated with Ti alloy coating, C_N = Coated with Ni coating, H_1 = First HIP cycle, and H_2 = Second HIP cycle.
(b) Coating peeled off after 128 cycles; test suspended.
(c) Test suspended.

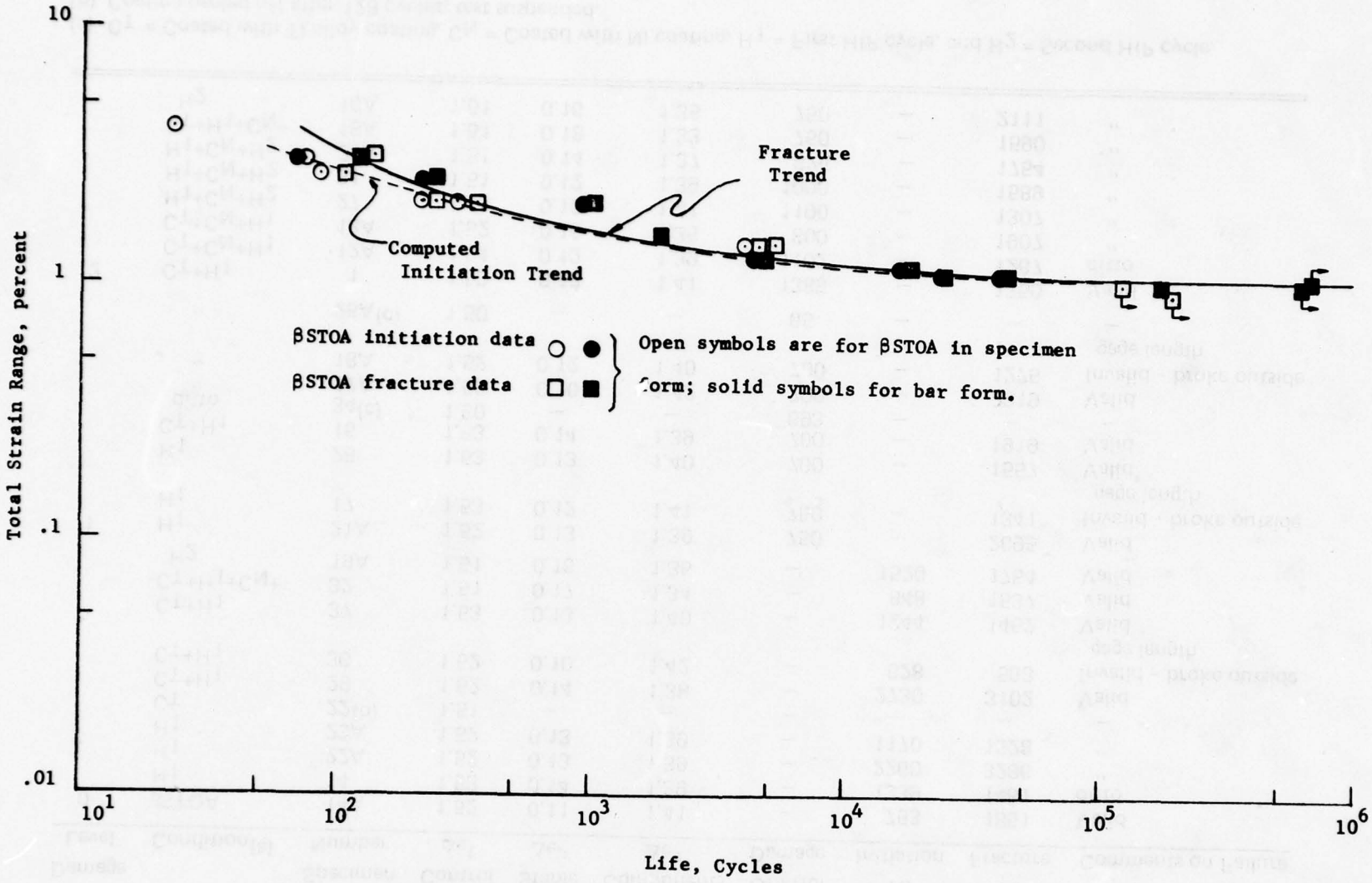

FIGURE 11. BASELINE PROPERTIES OF Ti-6Al-4V IN THE βSTOA CONDITION PRESENTED ON THE BASIS OF TOTAL STRAIN RANGE

200 cycles for a stress range corresponding to a total strain range of 1.5 percent is in reasonable agreement with the experimentally observed average value noted above and shown in Figure 11. This is significant in that it indicates the back extrapolated value of initiation includes only very few propagation cycles. The corresponding computed value of N_i/N_f of about 80 percent compares closely with the trend of 0.86 shown previously in Figure 10a.

The above crack propagation period has been computed via an approximate integration of the Paris[7] rate equation assuming (1) the crack is closed in compression under fully reversed loading, (2) the effective stress intensity is given by $K_{eff} = (1-R)^{1/2} K_{max}$ where R is the algebraic ratio of the minimum to maximum stress intensity ratios and K_{max} is the maximum stress intensity, (3) the threshold stress intensity is K_{th} = 12.5 ksi $\sqrt{\text{in.}}$ so that the crack size (depth) corresponding to crack initiation is 0.005 in., and (4) the critical stress intensity, K_c = 140 ksi $\sqrt{\text{in.}}$ so that the crack size (depth) for unstable growth is 0.15 in. The stress intensity, K, has been assumed to be related to the current crack depth, a, through the approximate relationship based on the modified surface flaw equation:

$$K = \frac{1.95\, s\, a^{1/2}\, \alpha d}{Q^{1/2}} \quad .$$

In this equation, s is the far field stress, α_d is an edge notch finite width correction and Q is the flaw shape parameter which is a function of the flaw width-to-depth ratio and the extent of crack tip inelastic action measured by the ratio s/s_y where s_y is the yield stress of the material. It should be pointed out that the computed crack propagation period can be shown to vary between 490 and 175 cycles by computing the period at the apparent extremes of the above noted average values of K_c and K_{th}. The average of these extremes is 332 cycles. Also, at the value of K_c listed above, the stable crack size is 0.15 in. deep and embraces about 30 percent of the circumference. In most of the specimens, it was difficult to distinguish the slow crack growth region on the fracture surface, but values comparable to these were observed in specimen Nos.1 and 2a. In Specimen No. 1 the corresponding values were 0.20 in. and 36 percent.

The data tabulated in Table 5 can also be graphically presented in the form of Figure 12 which plots log plastic strain range versus log life. This form tends to "spread out" the data shown previously in Figure 11 on the basis of total strain range. As in Figure 11, data are plotted for both initiation and separation and a trend line is shown for the experimentally measured separation life. This plastic strain-life to separation line has been established giving consideration to three major factors: (1) the distribution of the fatigue failure data, (2) the value of the true fracture strain range (0.228 of the true fracture strain measured from a tensile test) through which the curve should pass, and (3) the characteristic slope of such Coffin-Manson plots. The chosen trend curve drawn in Figure 12 has a slope of about -0.5, almost passes through the

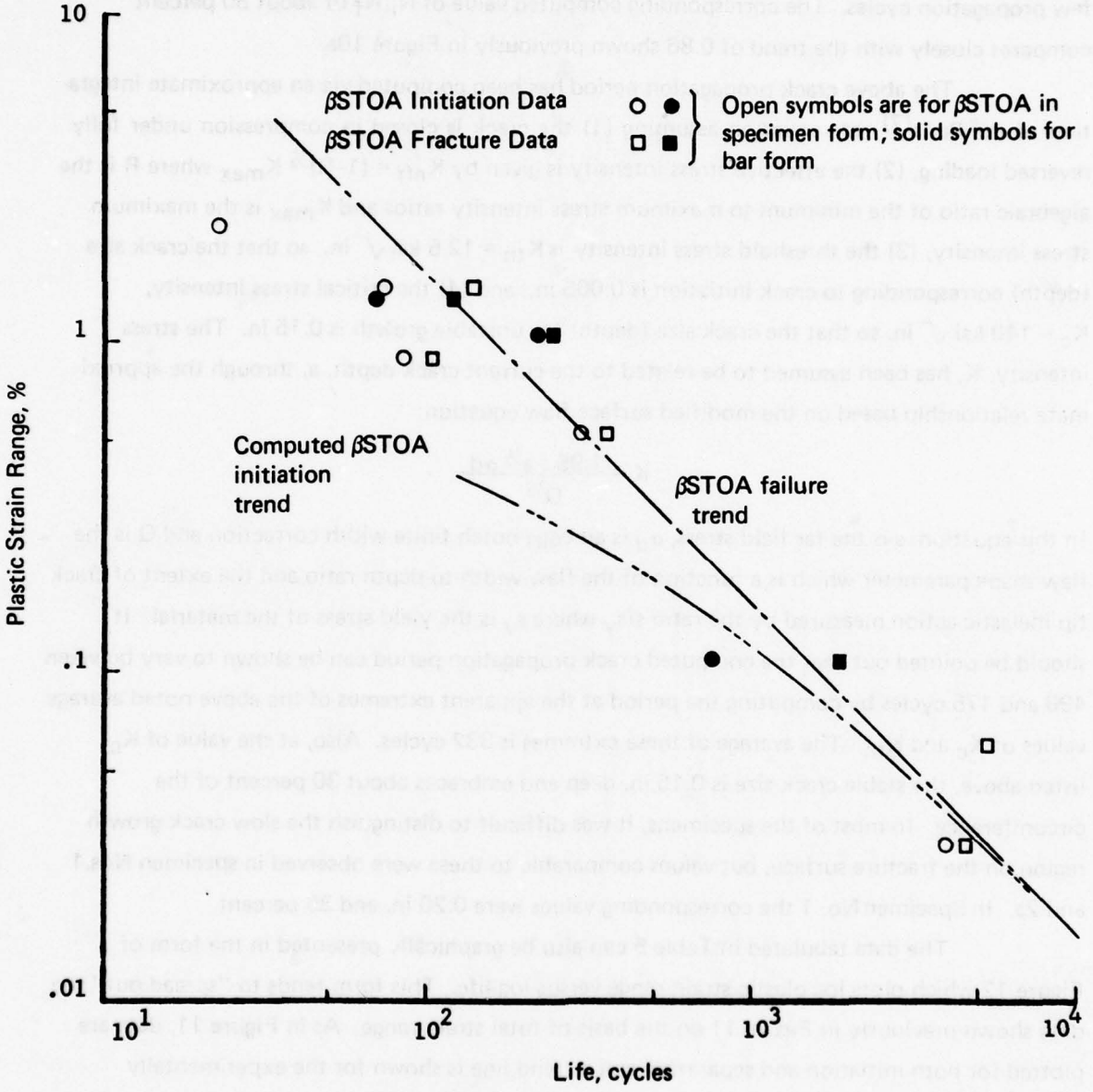

FIGURE 12. BASELINE PROPERTY DATA PRESENTED ON THE BASIS OF PLASTIC STRAIN RANGE

true fracture strain*, and provides a reasonable fit through the failure data without encompassing any of the initiation data at lives to crack initiation greater than 100 cycles, except for one long life point. Also as in Figure 11, a trend curve corresponding to crack initiation based on the measured failure data and a constant crack propagation period of 332 cycles (consistent with the trend in the value of N_i/N_f of Figure 10) is shown in this figure. Note that this value of 332 cycles corresponds closely with the average value of the propagation period for baseline data of 371 cycles. Note also that this trend seems to provide a reasonable fit to the initiation data.

Data from Table 8 for the predamaged specimens (Levels 1 and 2) can also be used to ascertain the life to crack initiation of the βSTOA material. The Level 1 predamage cycles serve as a lower bound on initiation material. The Level 1 predamage cycles serve as a lower bound on initiation whereas the Level 2 predamage cycles provide an upper bound on initiation. Note that "initiation" in these data was defined in terms of specimen compliance in a manner consistent with the back extrapolation of the asymmetric tensile load drop-off introduced previously. The samples at Level 1 damage showed no evidence of surface cracking by visual inspection at 30X magnification. While the Level 2 specimens did have surface cracks, the samples at higher cycle numbers contained more cracks of larger sizes than those at lower cycle numbers. Comparing these data to the initiation trend curve of Figure 12 as shown in Figure 13 indicates the validity of the initiation trend curve based on a constant propagation period of 332 cycles. The corresponding values of the ratio N_i/N_f for the extremes in failure data also compare well with the experimental values as shown in Figure 10.

Although all Level 1 and 2 predamage was imposed at nominally the same total strain range (1.50 percent), the plastic strain component varied significantly from test to test. Consequently, the relative predamage level varied from test to test (Figure 13) even though the number of predamage cycles may have been identical. This variability must be accounted for later in assessing the relative merits of HIP rejuvenation. Otherwise the true data trends may be masked (in an absolute sense) by the scatter in the rate of fatigue damage accumulation due to differing levels of plastic strain range in the individual tests.

The plastic strain-life format is also useful in assessing the influence of the HIP rejuvenation steps on the fatigue resistance of samples tested under total strain control at a nominal range of 1.50 percent. Pertinent data from Table 8 as plotted in Figure 14 along with the βSTOA trends (from Figure 11) show, in every case, that their fatigue resistance is superior. Yet, from part b of Figure 10, the corresponding values of the ratio N_i/N_f do not differ substantially from the βSTOA trend. If N_p is assumed constant, as discussed earlier, the improved fatigue resistance would be due to improvements only in the crack initiation resistance, i.e., increases in N_i.

* The point for true fracture strain is not included in Figure 12, but lies off to the left.

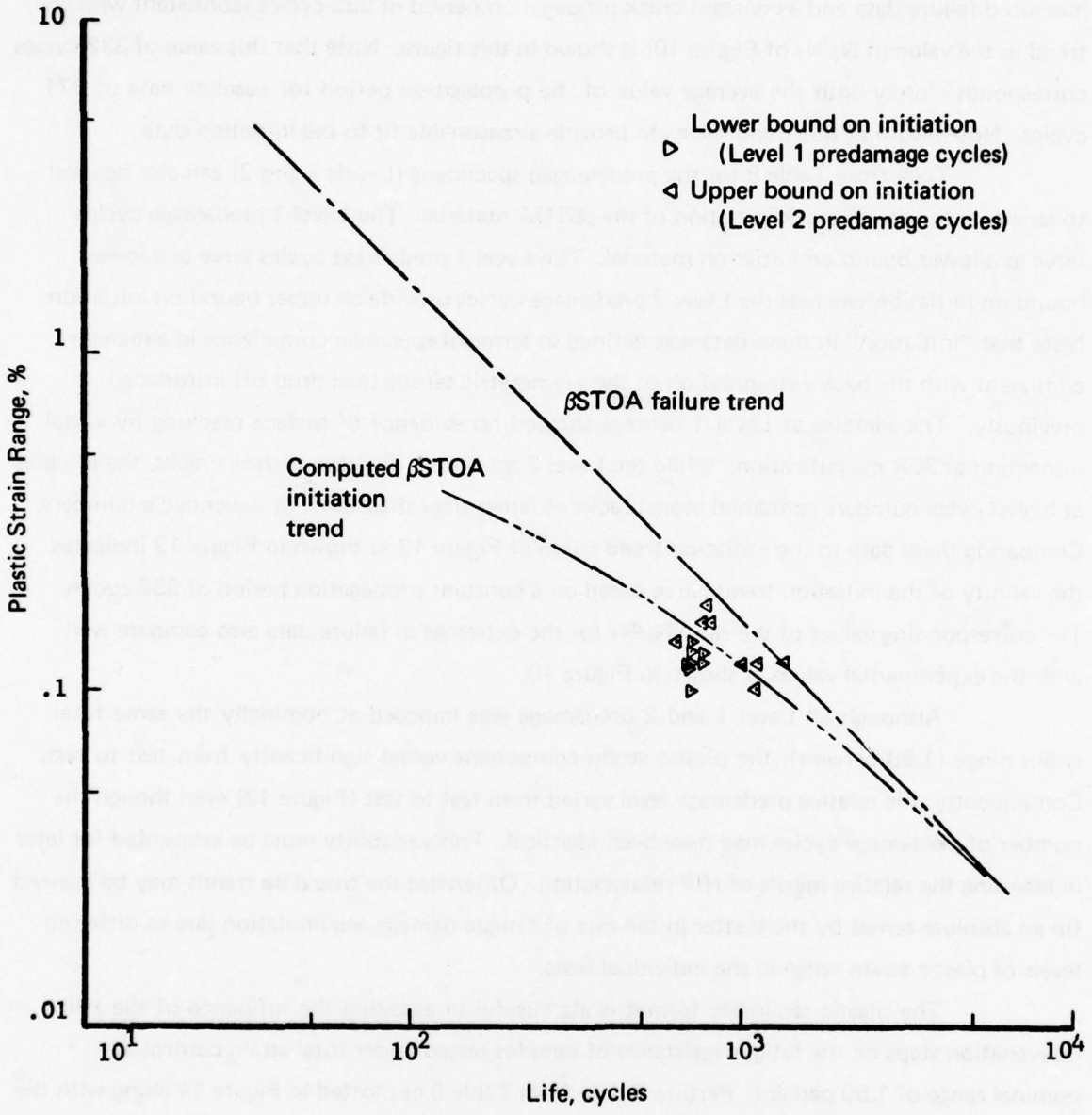

FIGURE 13. COMPARISON OF PREDAMAGED SPECIMEN PROPERTIES TO THE INITIATION TREND CURVE

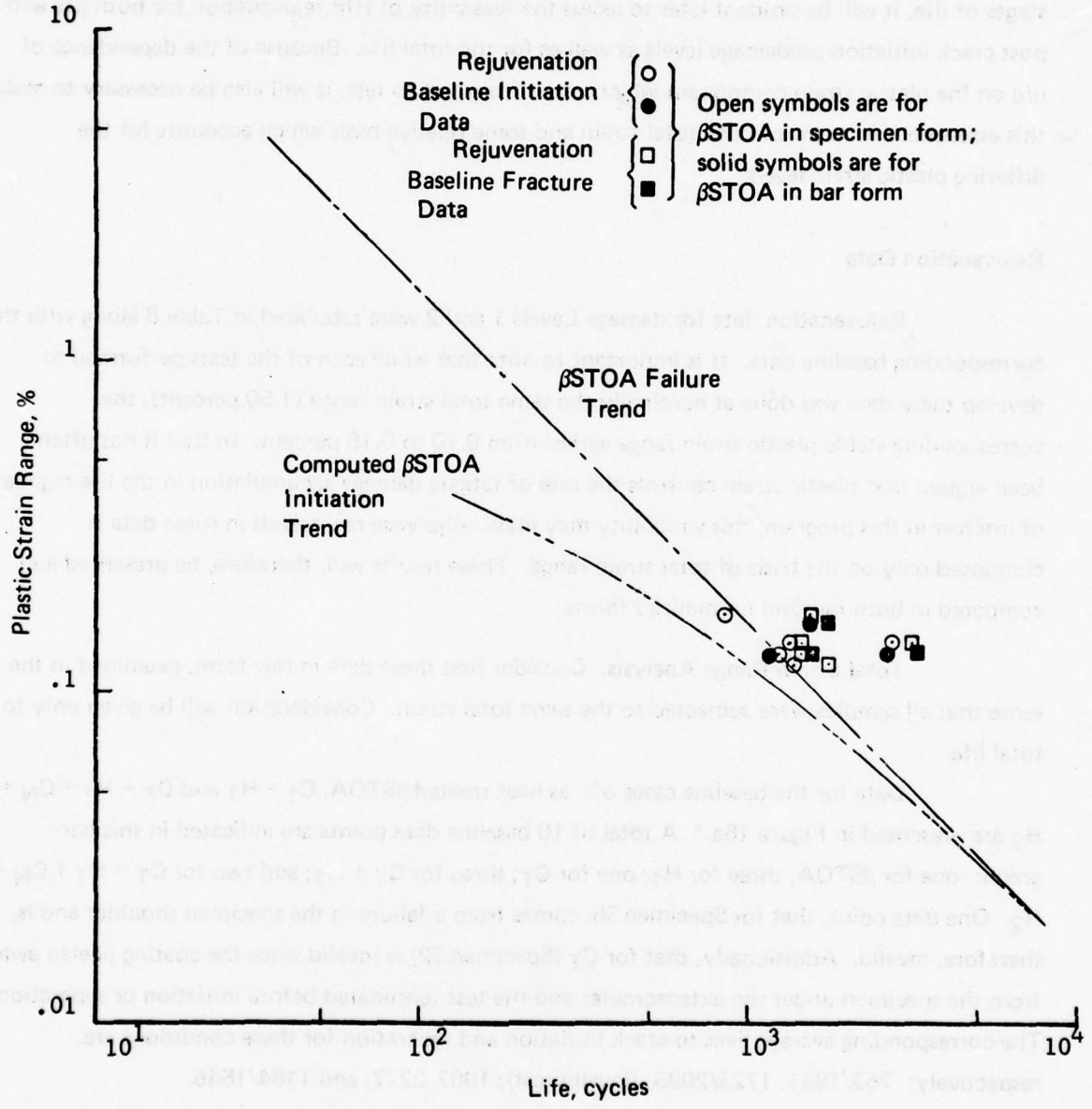

FIGURE 14. COMPARISON OF FATIGUE CRACK INITIATION AND FRACTURE BEHAVIOR OF βSTOA MATERIAL WITH MATERIAL SUBJECTED TO THE VARIOUS REJUVENATION PROCESS STEPS

Given that this assumption is true, the life to separation for baseline specimens subjected to the HIP process parameters, when normalized based on life to crack initiation, should closely correspond to the βSTOA trend. Figure 15 shows such a comparison and indeed indicates a close correspondence.

Because the rejuvenation steps apparently influence the initiation but not propagation stages of life, it will be prudent later to assess the feasibility of HIP rejuvenation for both pre and post crack initiation predamage levels as well as for the total life. Because of the dependence of life on the plastic strain component which varies from test to test, it will also be necessary to make this assessment in terms of both total strain and some relative basis which accounts for the differing plastic strain levels.

Rejuvenation Data

Rejuvenation data for damage Levels 1 and 2 were tabulated in Table 8 along with the corresponding baseline data. It is important to note that while each of the tests performed to develop these data was done at nominally the same total strain range (1.50 percent), the corresponding stable plastic strain range varied from 0.10 to 0.18 percent. In that it has often been argued that plastic strain controls the rate of fatigue damage accumulation in the life regime of interest in this program, this variability may mask otherwise real trends in these data if composed only on the basis of total strain range. These results will, therefore, be presented and compared in both raw and normalized forms.

Total Strain Range Analysis. Consider first these data in raw form; examined in the sense that all samples were subjected to the same total strain. Consideration will be given only to total life.

Data for the baseline cases of: as heat treated βSTOA, $C_1 + H_1$ and $C_T + H_1 + C_N + H_2$ are presented in Figure 16a.* A total of 10 baseline data points are indicated in this bar graph: one for βSTOA; three for H_1; one for C_T; three for $C_T + H_1$; and two for $C_T + H_1 + C_N + H_2$. One data point, that for Specimen 36, comes from a failure in the specimen shoulder and is, therefore, invalid. Additionally, that for C_T (Specimen 22) is invalid since the coating peeled away from the specimen under the extensometer and the test terminated before initiation or separation. The corresponding average lives to crack initiation and separation for these conditions are, respectively: 753/1851; 1723/2095; (invalid test); 1987/2277; and 1184/1645.

Note that for the βSTOA case, only one valid data point exists; that for Specimen 14A. Such a circumstance is hardly satisfactory in that only this single specimen forms the basis

* H_1 and H_2 refer to the first and second HIP cycles respectively. C_T indicates specimen was coated with Ti alloy coating and C_N indicates specimen was coated with Ni coating.

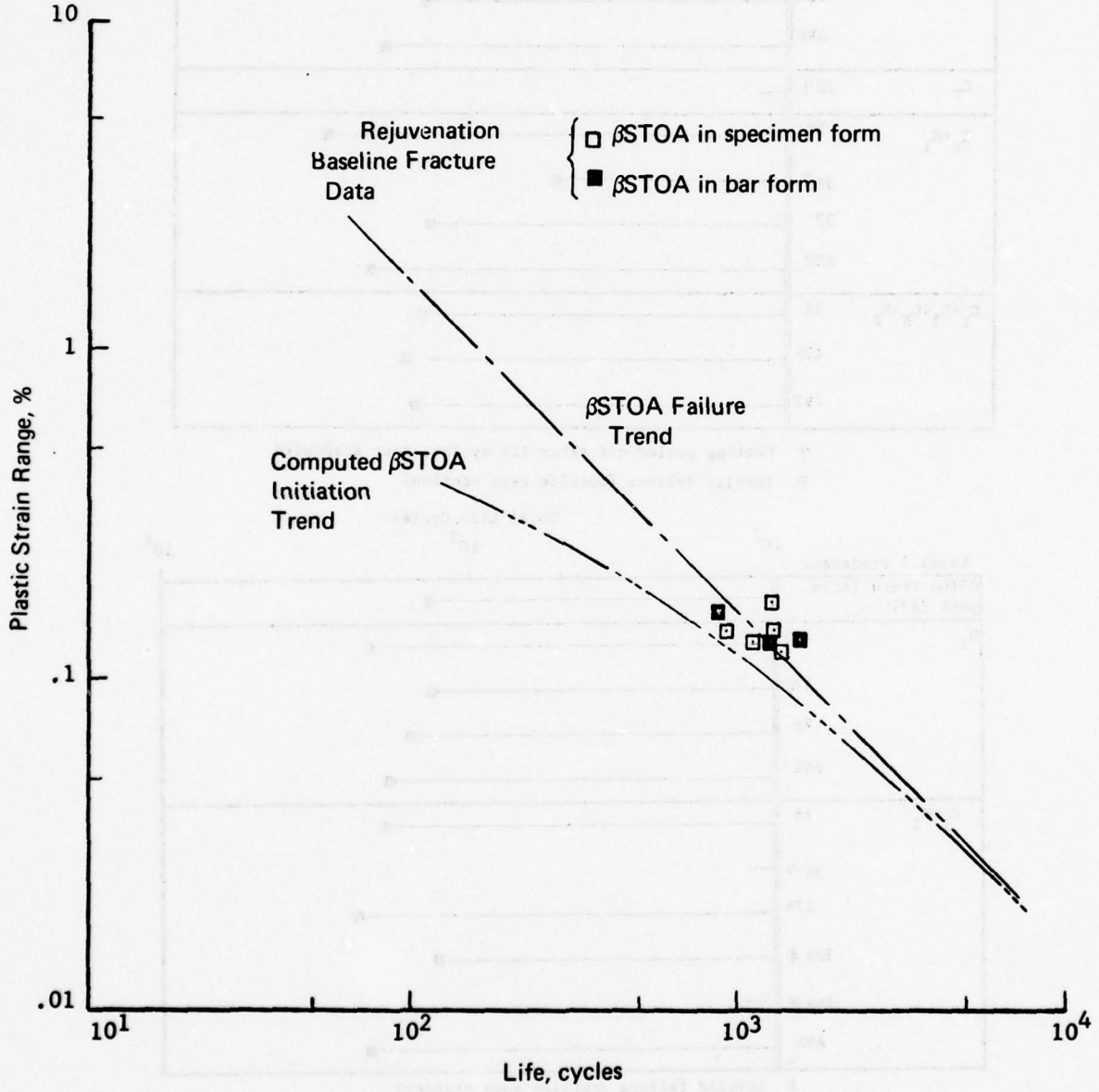

FIGURE 15. COMPARISON OF FRACTURE BEHAVIOR OF βSTOA MATERIAL WITH MATERIAL SUBJECTED TO THE VARIOUS REJUVENATION PROCESS STEPS AFTER NORMALIZATION BASED ON CRACK INITIATION

a.

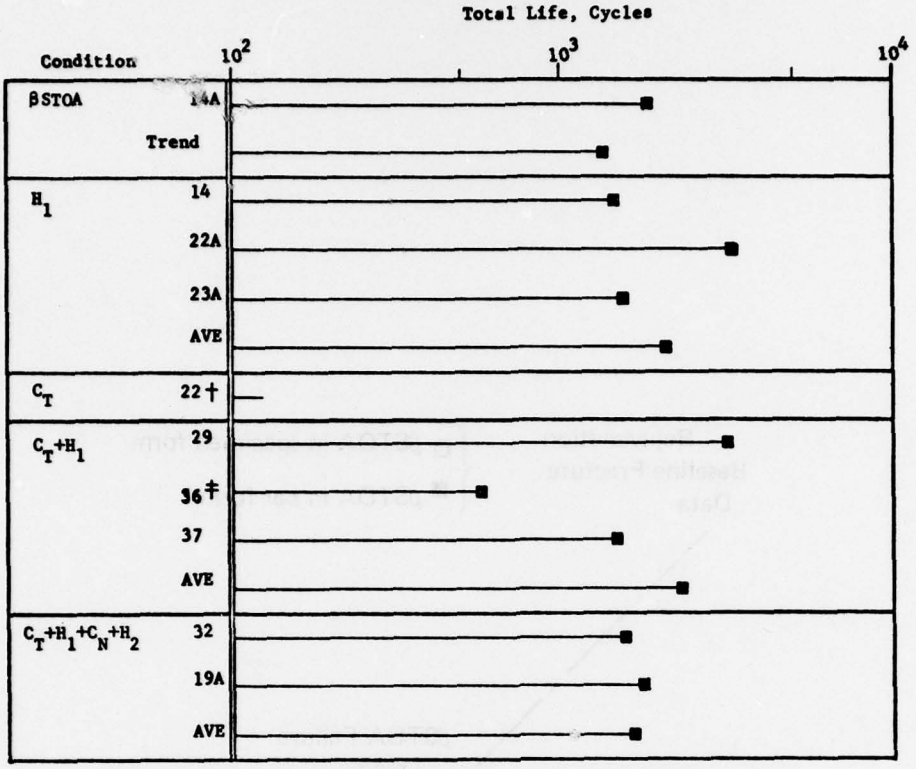

† Coating peeled off after 128 cycles; test suspended

‡ Invalid failure (outside gage section)

b.

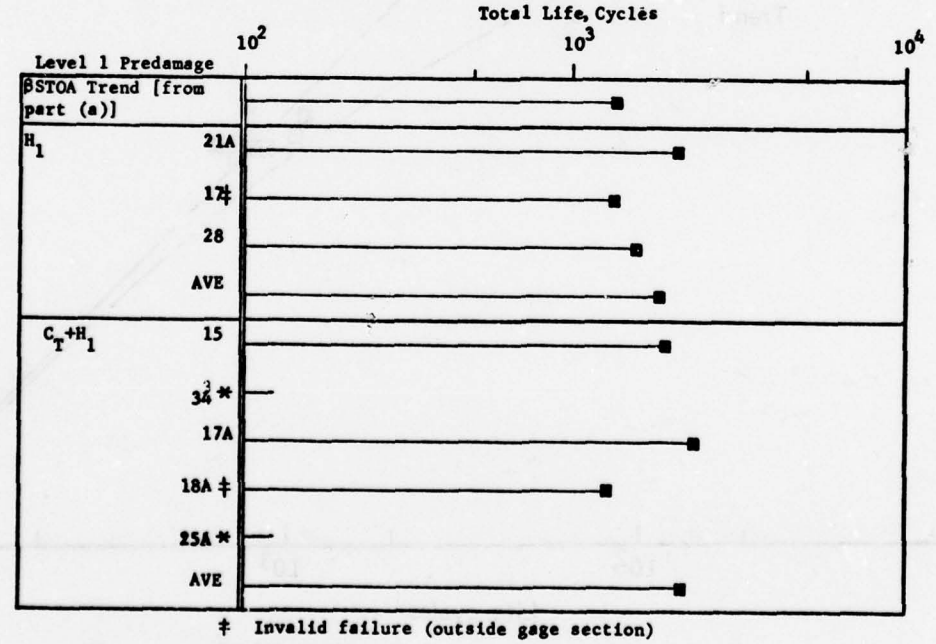

‡ Invalid failure (outside gage section)

* Test suspended

FIGURE 16. COMPARISON OF THE TOTAL FATIGUE LIFE OF THE βSTOA MATERIAL WITH THAT OF THE MATERIAL AFTER PREDAMAGE AND REJUVENATION BASED ON TOTAL STRAIN: PART a, BASELINE; PART b, LEVEL 1; PART c, LEVEL 2

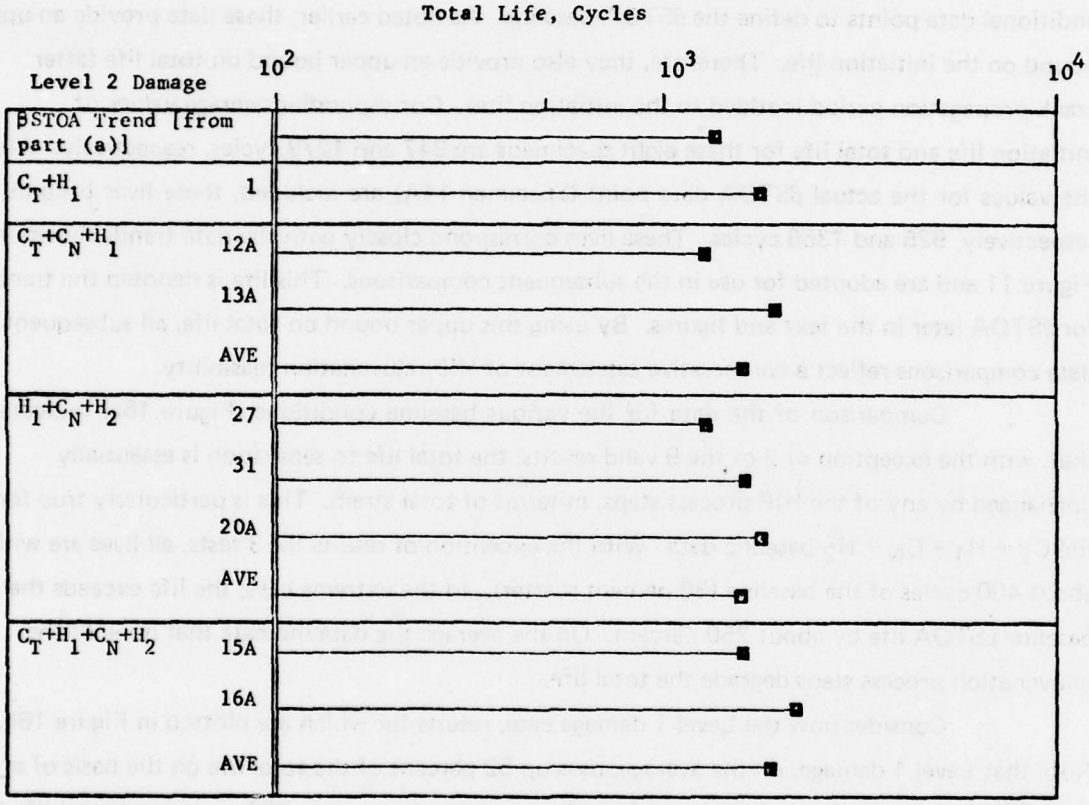

c.

FIGURE 16. COMPARISON OF THE TOTAL FATIGUE LIFE OF THE βSTOA MATERIAL WITH THAT OF THE MATERIAL AFTER PREDAMAGE AND REJUVENATION BASED ON TOTAL STRAIN: PART a, BASELINE; PART b, LEVEL 1; PART c, LEVEL 2

for all subsequent comparisons. To augment this data base or provide support for its use or modification, data representative of this baseline case developed in other stages of this program have been examined. That for the Level 2 predamage case seem most appropriate since at least the crack initiation stage (on the average 86 percent of the total life in these specimens) has been accomplished in the βSTOA state. (Note that here the measure of life to crack initiation is taken as the number of predamage cycles to develop Level 2 damage.) This life to crack initiation when coupled with a propagation period (previously assumed constant at 332 cycles) provides eight additional data points to define the βSTOA baseline. As noted earlier, these data provide an upper bound on the initiation life. Therefore, they also provide an upper bound on total life (after crack propagation period is added to the initiation life). Corresponding average values of initiation life and total life for these eight specimens are 947 and 1279 cycles, respectively. When the values for the actual βSTOA data point (Specimen 14A) are included, these lives become, respectively, 925 and 1358 cycles. These lives correspond closely with the data trends shown in Figure 11 and are adopted for use in the subsequent comparisons. This life is denoted the trend for βSTOA later in the text and figures. By using this upper bound on total life, all subsequent data comparisons reflect a conservative assessment of HIP rejuvenation feasibility.

Comparison of the data for the various baseline conditions (Figure 16a) indicates that, with the exception of 2 of the 9 valid results, the total life to separation is essentially unchanged by any of the HIP process steps, in terms of total strain. This is particularly true for the $C_T + H_1 + C_N + H_2$ baseline data. With the exception of results for 3 tests, all lives are within about 400 cycles of the baseline (30 percent scatter). In the extreme case, the life exceeds the baseline βSTOA life by about 250 percent. On the average the data indicate that none of the rejuvenation process steps degrade the total life.

Consider now the Level 1 damage case, results for which are plotted in Figure 16b. Note that Level 1 damage, on the average, uses up 52 percent of the total life on the basis of a Miner[8] linear damage rule (i.e., Level 1 predamage is on the average 706 cycles and total life for βSTOA is on the average 1358 cycles so that the predamage percentage is 706/1358 x 100%). Thus, if 100 percent rejuvenation occurred, the total life would be 1.52 x 1358 = 2064 cycles. Results presented in this figure show that, in some specimens, this level of rejuvenation is achieved for both H_1 and $C_T + H_1$ cases. On the average, H_1 achieves 1826 cycles for a net gain of 468 cycles or 468/679 x 100% = 69 percent of the maximum possible extension in life. Corresponding computations for the $C_T + H_1$ case show, on the average, a total of 2119 cycles for a net gain of 761 cycles. This indicates 112 percent of the maximum possible life extension has been achieved in this case. Scatter*, of course, gives rise to the excess of improvement over that theoretically

* Scatter is discussed later in this section.

expected. These results, therefore, indicated the feasibility of HIP rejuvenation for Level 1 damage. The H_1 results suggest that the thermal portion of the HIP cycle produces a substantial fraction of the new improvement (about 70 percent) through thermal and possibly pressure induced changes in the microstructural fatigue damage. The remainder of the potential improvement ($C_T + H_1$ versus H_1) is apparently due to the smoothing out of surface roughening and slip steps in coated specimens through the diffusion bonding of the compatible coating with the substrate as shown in the results of the metallographic studies. A consequence of this fact is that a compatible coating appears necessary for the mechanical portion of the HIP process to alleviate the surface related fraction of Level 1 damage.

Finally, consider results for Level 2 predamage as plotted in Figure 16c. Included in this figure are results for eight specimens obtained for four rejuvenation conditions, respectively: 1 for $C_T + H_1$; 12A and 13A for $C_T + C_N + H_1$; 27, 31, and 20A for $H_1 + C_N + H_2$; and 15A and 16A for $C_T + H_1 + C_N + H_2$. Note that Level 2 damage uses up, on the average, 70 percent of the total life on the basis of a linear damage rule (i.e., the average number of Level 2 predamage cycles is 947 whereas the average life to separation is 1358 cycles). Thus, if 100 percent rejuvenation occurred, the maximum total life would be 1.70 x 1358 = 2309 cycles. Clearly, 100 percent rejuvenation is not indicated by these data. Indeed, in two cases (Specimens 12A and 27) the HIP rejuvenation process proved slightly detrimental. Metallography performed on Specimen 12A (reported and discussed in detail later) indicates that the fatigue crack that propagated to failure in this sample was one of those present before rejuvenation. Therefore, it is likely that this crack has not been healed (because of bridging problems) so that its total life should and does correspond closely with the baseline βSTOA case (cf. 1267 and 1358). Unfortunately, similar metallographic results are not available for Specimen 27. It must therefore be assumed, because its life (1307 cycles) corresponds so closely with the βSTOA case, that it too failed at an unhealed crack. The remainder of the data all show evidence of rejuvenation. On the average (including 12A and 27), the results indicate 32 percent of the maximum possible rejuvenation is achieved. When 12A and 27 are excluded from the feasibility assessment, the results indicate that 45 percent of the maximum rejuvenation has been attained. In the three cases for which metallography indicates previously mapped cracks did not lead to failure (Specimens 13A, 16A, and 20A), an average of 60 percent of the maximum rejuvenation is not attained since, as shown later in the metallographic results, all bridged cracks in a given specimen may not have healed completely. Without complete healing, it is impossible to achieve the maximum potential rejuvenation. But even with the incomplete healing, these raw data indicate the feasibility of HIP rejuvenation of surface-connected fatigue cracking.

Plastic Strain Range Analysis. Consider next an assessment of the feasibility of HIP rejuvenation in terms of plastic strain, rather than total strain. Recall from the discussion of the baseline data that plastic strain provides a better basis for the assessment because its magnitude controls the rate of damage accumulation in the range of life of interest herein. Note that if the plastic strain component would have been constant from test to test like the total strain, the ensuing assessment would yield the same results as that based on total strain. However, because the plastic strain component varied from 0.10 to 0.18 percent, the subsequent assessment will give rise different results. Note also that the previous assessment failed to account for the influence of the HIP process parameters on the respective baseline fatigue resistances and is, therefore, biased. The ensuing assessment accounts for this aspect by comparing all results to a normalized baseline developed assuming (1) the predamage done in the βSTOA condition transforms into an equivalent amount of predamage in a HIP process baseline condition following a linear crack initiation damage accumulation rule and (2) a constant crack propagation period. Recall that the first assumption constitutes the often invoked Miner's rule[8] and that the second assumption is strongly supported by all data assembled and discussed previously.

For purposes of this assessment, trend curves for each of the baseline conditions other than βSTOA (i.e., H_1, $C_T + H_1$, $C_T + H_1 + C_N + H_2$) must be developed from data shown in Figure 14. Trend curves for total life have been obtained by assuming (1) that their respective Coffin-Manson slopes are identical to that for the βSTOA data, (2) data for a given condition and plastic strain level average arithmetically and (3) data for a given condition and different plastic strain ranges average logrithmically on both plastic strain and life. The resulting trend curves are shown in Figure 17.

Results obtained after the application of the normalization scheme outlined above are presented in Figure 18. Note that baseline data exist for the H_1, $C_T + H_1$, and $C_T + H_1 + C_N + H_2$ rejuvenation process steps. Thus, baseline data exist for all of the Level 1 conditions and two of the four Level 2 conditions. Baseline data for the remaining Level 2 conditions have been approximated by available data. For the $C_T + C_N + H_1$ data the baseline has been approximated by $C_T + H_1$ data; while for the $H_1 + C_N + H_2$ data the baseline has been approximated by $C_T + H_1 + C_N + H_2$ data. (Note that less than 2 percent difference exists between the results shown for the $C_T + C_N + H_1$ data and that obtained when the baseline is approximated by $C_T + H_1 + C_N + H_2$ data.) It is clear from this figure that HIP rejuvenation of both Level 1 and Level 2 surface-connected fatigue damage is feasible.

In contrast to the examination of the data in raw form on a total strain basis which indicates an effective rejuvenation for Level 1 damage after H_1 and $C_T + H_1$ as 69 and 112 percent, respectively, the normalized format indicates these rejuvenation's steps are 15 and 33

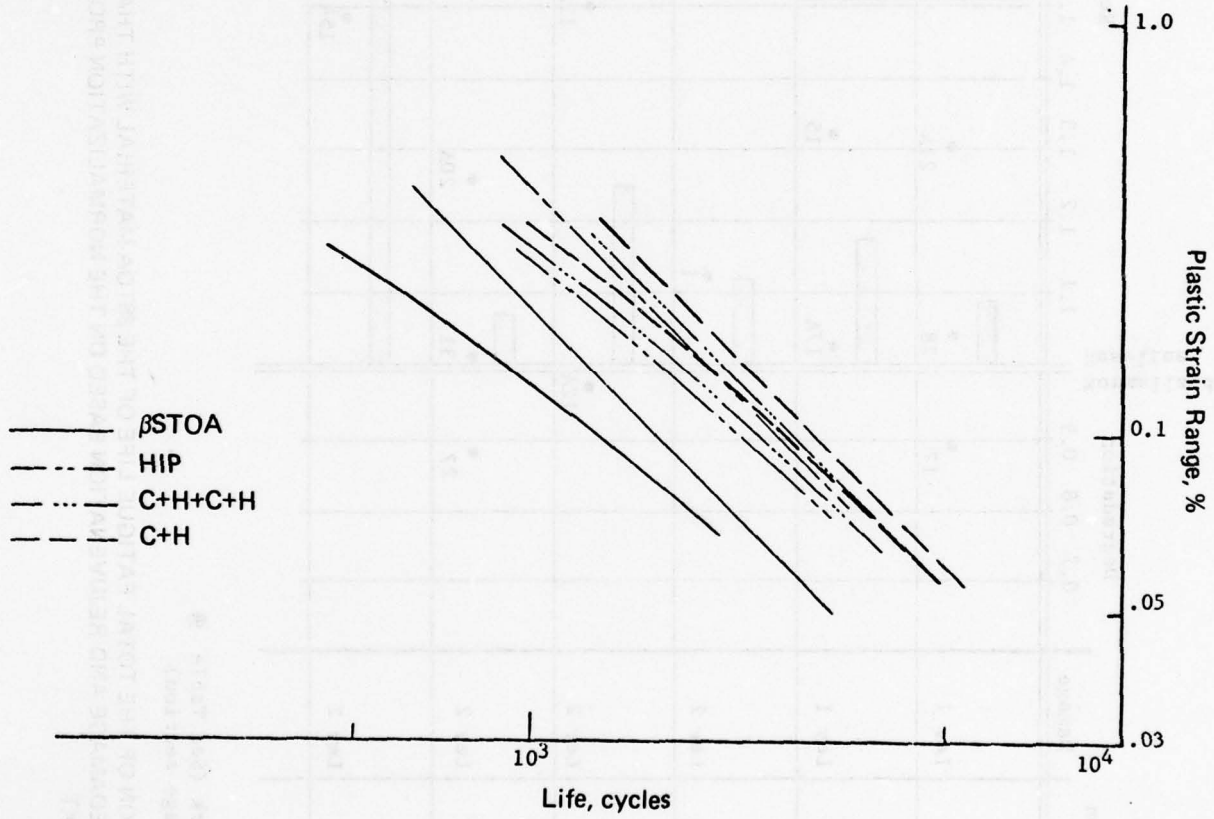

FIGURE 17. AVERAGE FATIGUE CRACK INITIATION AND FRACTURE BEHAVIOR OF THE βSTOA MATERIAL AND MATERIAL SUBJECTED TO THE VARIOUS REJUVENATION PROCESS STEPS

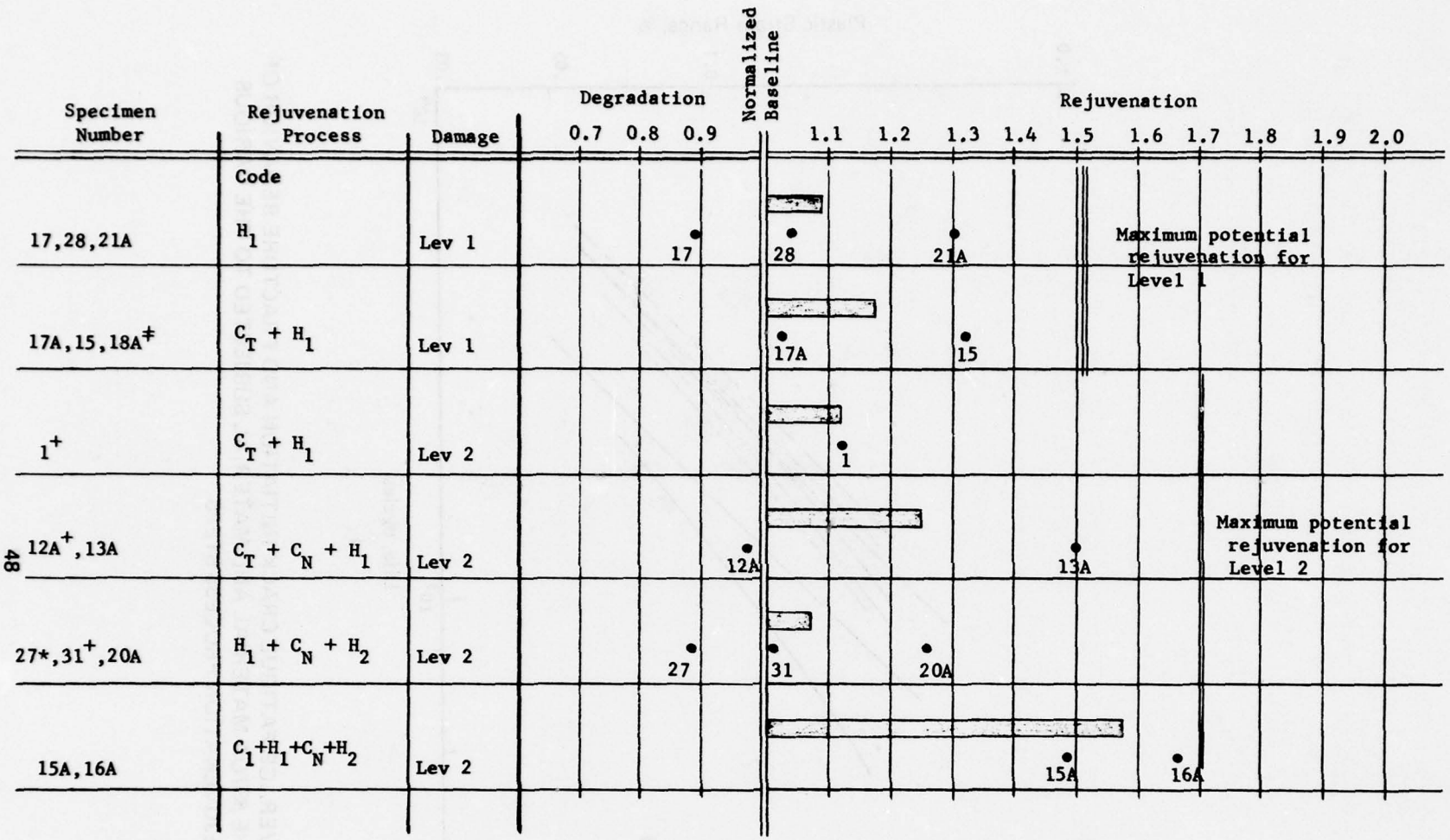

* No metallography
\+ Failure at an existing crack (See Table 9)
‡ Invalid failure (outside gage section)

FIGURE 18. COMPARISON OF THE TOTAL FATIGUE LIFE OF THE βSTOA MATERIAL WITH THAT OF THE MATERIAL AFTER PREDAMAGE AND REJUVENATION BASED ON THE NORMALIZATION PROCEDURE DETAILED IN THE TEXT

percent effective. Thus, it shows the same trends but indicates a substantially lower level of rejuvenation. Inspection of the data indicates that this difference in the level of rejuvenation can be attributed to the use of (1) baseline βSTOA data with an average life to separation substantially less than that of the baseline data for each of the rejuvenation process conditions and (2) baseline βSTOA data for an assumed constant value of the plastic strain range (~ 0.125 percent) when the value actually ranged from 0.10 to 0.18 percent. These same differences do not, however, impact strongly on the relative effectiveness of rejuvenation for Level 2 as assessed in terms of either raw or normalized data because both formats utilize a common, constant, measure of the crack propagation period (i.e., both assume it to be 332 cycles). For example, for the three specimens for which metallography indicates previously mapped cracks do not lead to post rejuvenation failure, the previous format shows the process to be 60 percent effective whereas the present indicates the process is 68 percent effective, on the average.

Regardless of which of the two data analyses formats is adopted, these data indicate the feasibility of HIP rejuvenation of both Level 1 and Level 2 fatigue damage. It should be noted that this feasibility has been demonstrated using non-optimized HIP or coating processes. It is, therefore, likely that the extent of rejuvenation can be substantially improved upon. In this same context, it should also be noted that the issue of feasibility may be somewhat clouded by scatter in the various data sets. A brief analyses of the influence of scatter follows.

Consider first the most extensive set of data developed in this program -- that for Level 2 predamage in the baseline βSTOA condition. These data are from Specimens 1, 27, 31, 12A, 13A, 15A, 16A and 20A and cover a range of crack sizes as noted later in Figure 21. In part, the scatter in the life indicative of the presence of Level 2 damage is due to this scatter in crack sizes. For this reason, at least Specimen 1 should not be considered in that it contained at least four observable cracks. For the remaining specimens, Level 2 damage has been observed respectively at 1100, 1000, 1102, 800, 750, 750, and 625 cycles; the average being 875 cycles with a computed population standard deviation of 176 cycles. Thus the scatter band is about ± 20 percent of the mean. When this scatter band is considered in terms of Figure 18, the normalized baseline is seen to range from 0.8 to 1.20 while the maximum rejuvenation for Levels 1 and 2 range, respectively, from 1.42 to 1.62 and 1.56 to 1.84. (More elegant and extensive consideration of the influence of scatter on the demonstration of feasibility may be desirous; they are, however, unwarranted, and, in some instances, impossible due to the limited data set generated in this program.)

Clearly, scatter alone is not responsible for the longer lives observed after rejuvenation of Level 1 and Level 2 damage. These data, therefore, demonstrate the feasibility of HIP processing to extend the life of βSTOA Ti-6Al-4V fatigue test specimens of the type used in this

program. These results should, however, not be construed as validation of the HIP rejuvenation process nor should they be considered indicative of the extent of rejuvenation possible after the process parameters have been optimized.

Fatigue Damage Characterization

The fatigue damage was studied by surface examination and longitudinal sectioning of fatigue specimens. One specimen was sectioned after fatigue testing short of failure to establish the sub-surface crack morphology, while several were sectioned after fracture. In addition, the surfaces of all of the specimens damaged to Level 2 were examined and the locations of all visible cracks (at 30 X) mapped before the surface was coated and subsequently HIP.

To assess the types of fatigue damage representative of this material, a specimen for metallographic characterization was subjected to extensive fatigue damage to introduce a large number of damage sites of different degrees of severity (23 cycles at a strain amplitude of 4 percent). The damage shown in Figure 19 would be typical of the precrack initiation stage, Level 1 damage. Surface offsets develop (Figure 19a), and cracks subsequently initiate at these sites and propagate along the interphase boundaries (Figure 19b). This was the most common mode of crack initiation, and other examples of cracks associated with surface offsets are shown in Figure 8a. In Figure 19c a short crack not associated with a surface offset is propagating normal to the surface and does not appear to be following an interphase boundary.

The upper layers in Figure 19 are the Ti-6Al-4V coating applied after fatigue but before metallographic sectioning. The cracks appear at the original specimen surface and extend into the specimen, and faults in the coating, extending up through the coating from the surface cracks or offsets, are visible in the figures.

Surface cracks representative of Level 2 damage, extending approximately 25 to 75 μm deep from the surface, are shown in Figure 20. These cracks, still in Stage I of crack growth, usually propagate along interphase boundaries, and the two cracks in Figure 20 lie parallel to the two intersecting sets of long narrow lamellae.

Characterization of the Level 1 damage on the individual predamaged specimens was outside the scope of this program. Level 2 damage in the form of cracks visible at 30 X magnification, were located by scanning the specimen surface before coating, and the shape and location for each crack was mapped for each Level 2 specimen except one (Specimen 27). Smaller cracks, if present, would have escaped observation and not be mapped.

Figure 21 shows representative cracks after cycling to increasing fractions of the fatigue life. The cracks do not propagate normal to the stress axis, but rather propagate in other directions dictated by the orientation of the underlying microstructure (Figure 20). The changes

500 X

a. Surface offset without crack

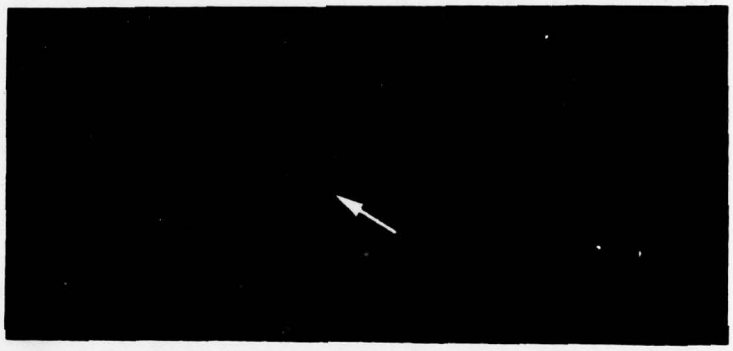

500 X

b. Surface offset with short crack

500 X

c. Short crack normal to surface

FIGURE 19. EARLY STAGE OF FATIGUE DAMAGE SHOWING FATIGUE CRACK NUCLEATION AT THE SPECIMEN SURFACE

The specimen was coated after fatigue and before sectioning, therefore the upper part in the micrographs is the Ti-6Al-4V coating and the lower part is the fatigue specimen. The cracks originate at the original specimen surface

100 X

FIGURE 20. SURFACE CRACKS SEEN ON A LONGITUDINAL SECTION

The cracks usually propagate along the interfaces of long lamellar as shown here.

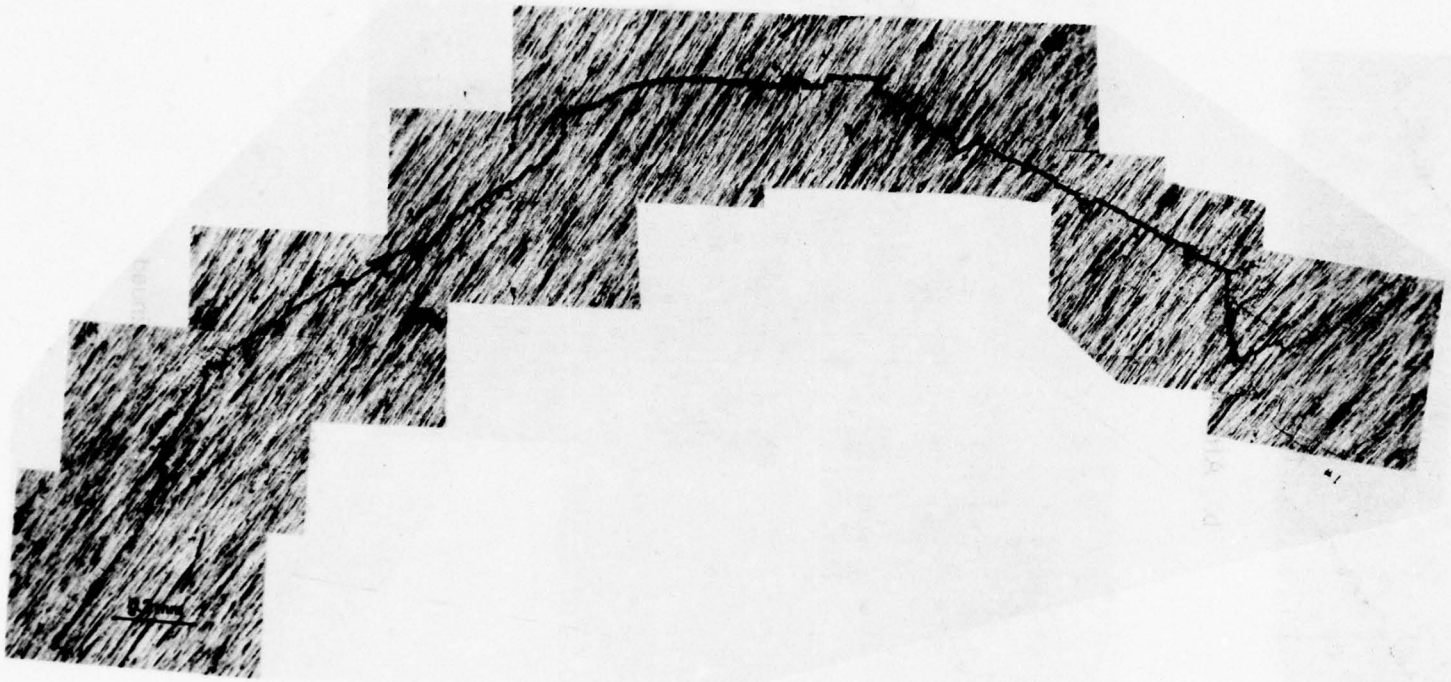

a. After 1450 cycles

FIGURE 21. SURFACE INTERSECTIONS OF FATIGUE CRACKS AFTER DIFFERENT NUMBERS OF CYCLES INTO LEVEL 2 DAMAGE AT A STRAIN AMPLITUDE OF 1.5 PERCENT

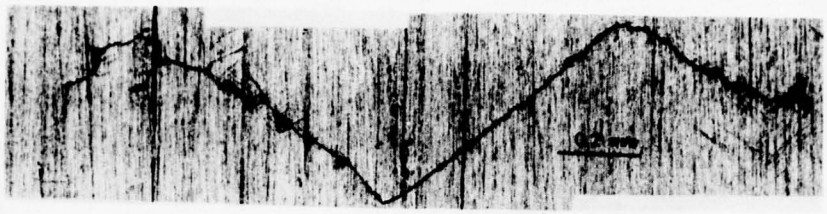

b. After 11 cycles

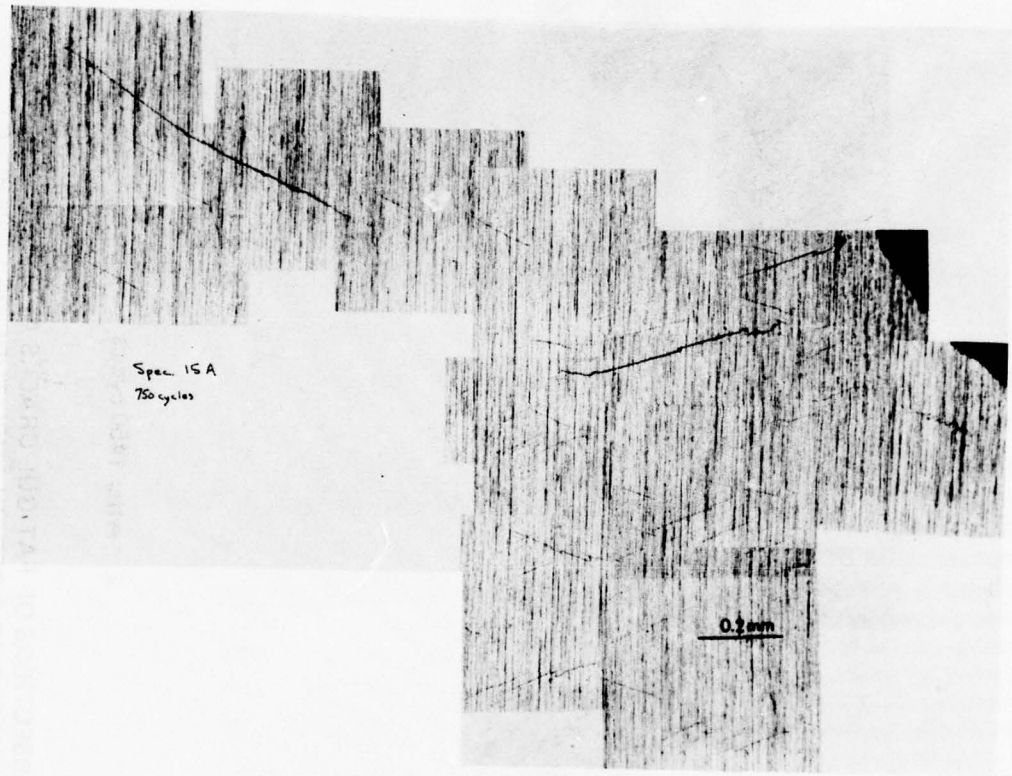

c. After 750 cycles

FIGURE 21. Continued

in direction occur over segment lengths on the order of the grain size and are probably due to neighboring grains having different orientations. The crack opening distance increases with increasing number of cycles (Figures 21a to 21c). Also, two configurations of cracks were observed, isolated single cracks (Figures 21a and 21b) and nests of fine cracks (Figure 21c). However, there was secondary cracking along some of the larger cracks and particularly at the ends of the larger cracks (Figures 21a and 21b).

The results of the surface observations of the Level 2 specimens are presented in Table 9 with the exception of Specimen 27 which was not examined before coating. The specimens having the highest number of cycles had the most individual visible cracks as well as the longest cracks, except that Specimens 15A and 20A each had an extensive group of small, neighboring cracks (Figure 21c).

Influence of HIP on Fatigue Damage

HIP would not close cracks open to the surface, therefore only coated specimens were examined after HIP. Unfortunately, the Ti-6Al-4V coating was unable to completely bridge most of the cracks, so these unbridged cracks were not healed. Evidence was found indicating that some cracks were closed and either completely or partially bonded, and therefore must have been bridged.

The appearance of the coating at a surface offset and at fatigue cracks after HIP is shown in Figure 22. There is a coating defect at the surface offset (Figure 22a) and the offset does not appear to be bonded to the coating. The cracks do not appear to be closed at all (Figure 22b); the crack opening probably is about the same as before HIP (Figure 20). Thus, since these cracks were not sealed over, no closure, much less bonding, could occur. Another example of an unbridged crack was presented in Figure 8b.

Further demonstration of the lack of crack healing was obtained by examining the surfaces of several Level 2 specimens following coating, HIP and fatigue to fracture. In each instance surface cracks were seen with the same shapes and in the same location as noted before coating. Thus these cracks had not been bonded and during subsequent fatigue testing after HIP they had opened back to the surface through the coating.

Evidence of crack healing was of two types. Indirect evidence was obtained by examining Level 2 specimens after final fracture for cracks which were present before coating, but did not reappear during the final fatigue testing. One case was found and successive sections taken through the region where the crack had been seen prior to coating, they failed to show them (Specimen 17). Considering the ease of showing up the cracks on longitudinal sections, (Figures 19 to 21), it is reasonable to conclude that the crack found had been completely bonded

TABLE 9. SUMMARY OF SURFACE OBSERVATIONS OF SPECIMENS SUBJECTED TO LEVEL 2 DAMAGE

Specimen Number	Number of Cycles Damage	Total Number of Cracks Detected	Maximum Crack Length, mm	Fractured at Existing Crack
1	1450	4	2.80	Yes
12A	1102	5	1.75	Yes[a]
13A	800	2	0.90	No
31	1000	2	0.90	Yes[a]
20A	625	Group	0.60	No
15A	750	Group	0.80	Possible
16A	750	1	–	No

(a) Not the longest crack measured on specimen surface.

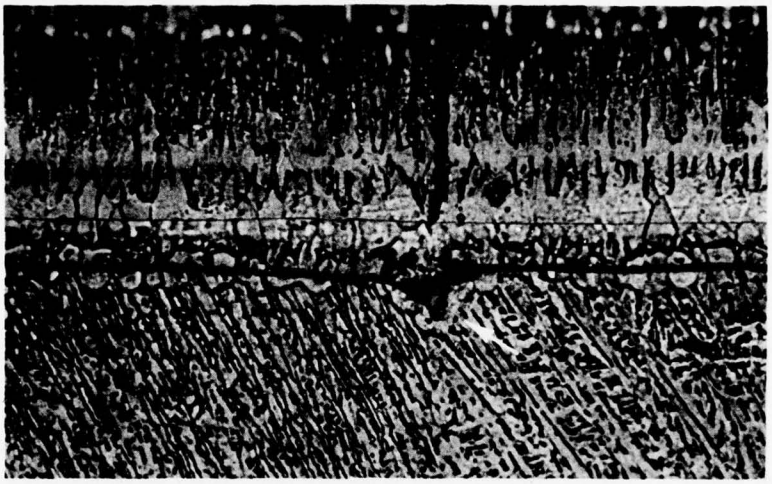

750 X

a. Fatigue-induced surface offset

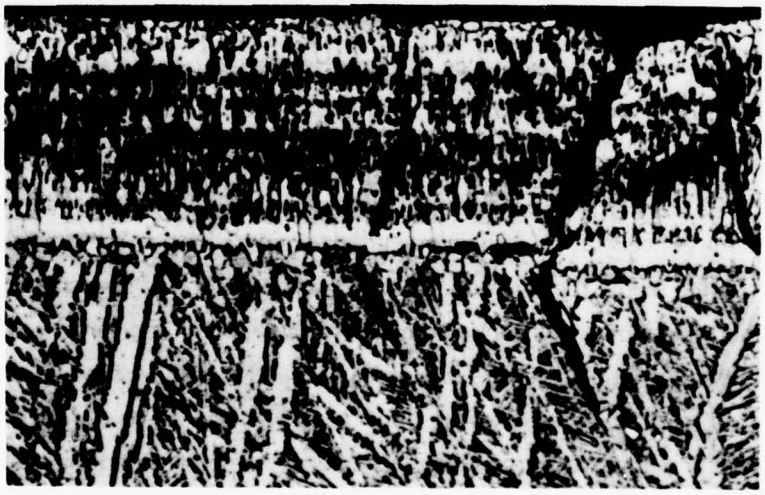

250 X

b. Fatigue cracks not completely covered by coating

FIGURE 22. APPEARANCE OF SURFACE OF FATIGUE-DAMAGED SPECIMEN AFTER COATING WITH Ti-6Al-4V PLUS HIP

together. Completely bonded cracks would be very difficult to identify because the cracks follow the interphase boundaries and don't create a discernable disturbance within the grain.

Direct evidence of crack bonding was obtained for a partially bonded crack in Specimen 20A. This specimen contained a small group of cracks after 625 fatigue cycles (Figure 23a). This specimen was then HIP without the Ti-6Al-4V coating, overcoated with nickel, again HIP and subsequently fatigue tested to failure. Surface examination after failure showed that the specimen failed near, but not within the initial group of cracks. However, there were cracks present in the region of Figure 23a after fatigue to fracture (Figure 23b), including a relatively large crack (Figure 24a). When this specimen was sectioned longitudinally through the larger crack (Figure 24a) the evidence for a partially bonded crack was found. The configuration of the partially bonded crack associated with the open crack is shown in Figure 24b, where the tip of the arrow marks the position of the partially-bonded crack, which is an extension of the lower, angled portion of the open crack. The original path of the crack is identified by a row of porosity caused by incomplete bonding. This porosity is shown in Figure 25a where the etched surface has been smoothed somewhat by polishing. The existence of the crack was verified by removing 0.5 mm from the surface and repolishing and etching. The partially bonded crack is still visable (Figure 26), but the two open cracks are now separated. Another 0.5 mm was removed with similar results, corroborating the existence of a long, partially bonded crack.

The original (partially bonded) crack has the appearance of the Stage I cracks shown earlier (Figures 20 and 22b); following interphase boundaries in from the surface. The new crack, initiated during final fatigue testing to failure, may have initiated in this location either because of the large concentration of previous fatigue damage here or the presence of the open crack segment located below the surface. After propagating into the specimen a short distance, it intersected the original partially bonded crack. However, it is not clear whether the original crack had partly bonded along its entire original length and subsequently reopened after the new crack impinged on it, or whether only the upper part had bonded as suggested by Figure 26.

There are at least two possible reasons for incomplete bonding of the crack in Specimen 20A (Figures 23 to 26). Firstly, the HIP conditions (time, temperature, pressure) might have been marginal for full crack closure and bonding in some cases, even if the cracks were bridged. Secondly, Specimen 20A was given a first HIP cycle without a coating (fulfilling a part of the original test matrix, Table 1). This might have induced some oxidation within the open cracks from the atmospheres during the first HIP cycle which inhibited bonding during the second HIP cycle after overcoating with nickel.

The light surface layer in Figures 24 to 26 is a thin layer of the nickel plating which was not completely removed after HIP. The dark region below the nickel plate is a high nickel

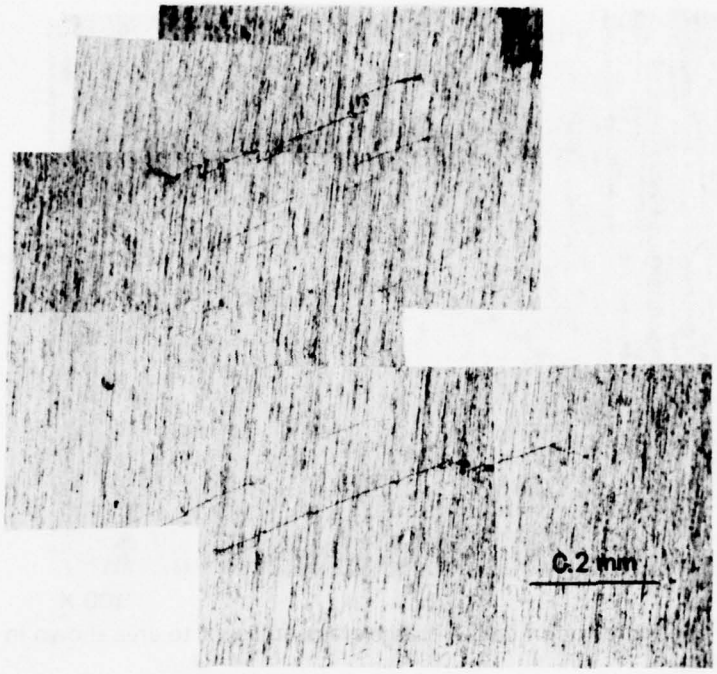

a. Group of cracks after 625 fatigue cycles

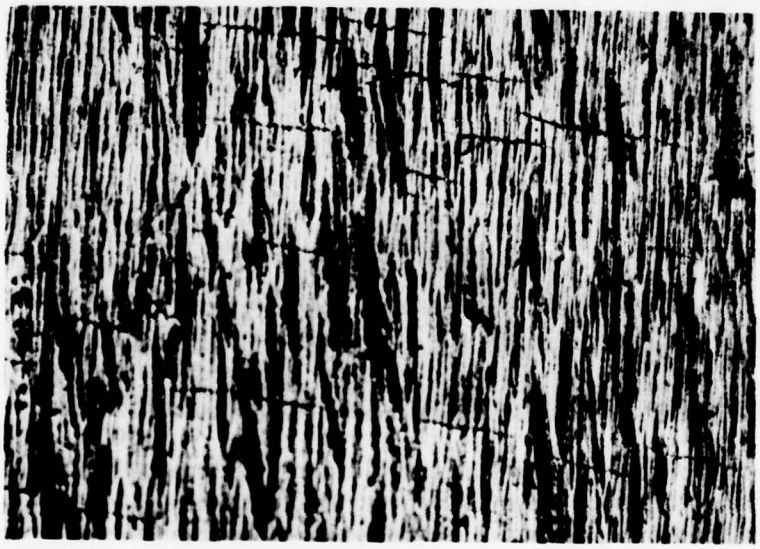

b. Group of cracks after coating, HIP and final fatigue fracture, same area as in (a) above

FIGURE 23. GROUP OF SURFACE CRACKS IN SPECIMEN 20A AFTER THE LEVEL 2 DAMAGE AND AFTER FINAL FATIGUE FAILURE

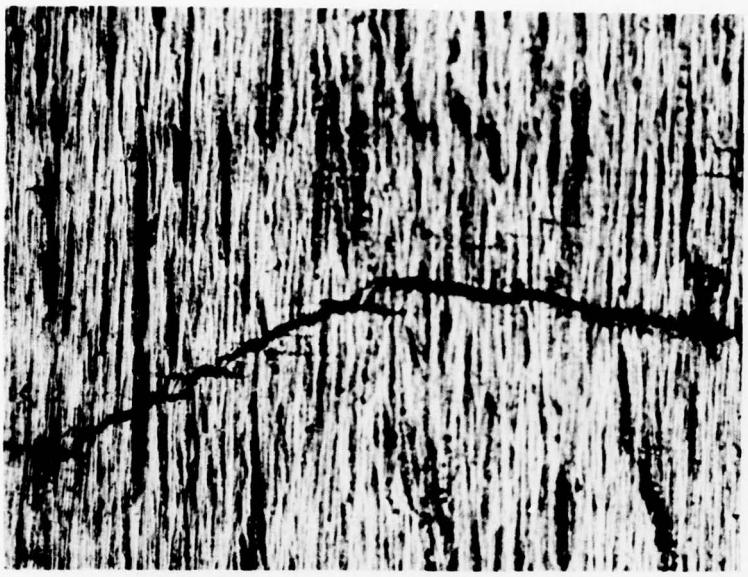

180 X

a. Surface configuration of crack. Large crack adjacent to area shown in Figure 10b.

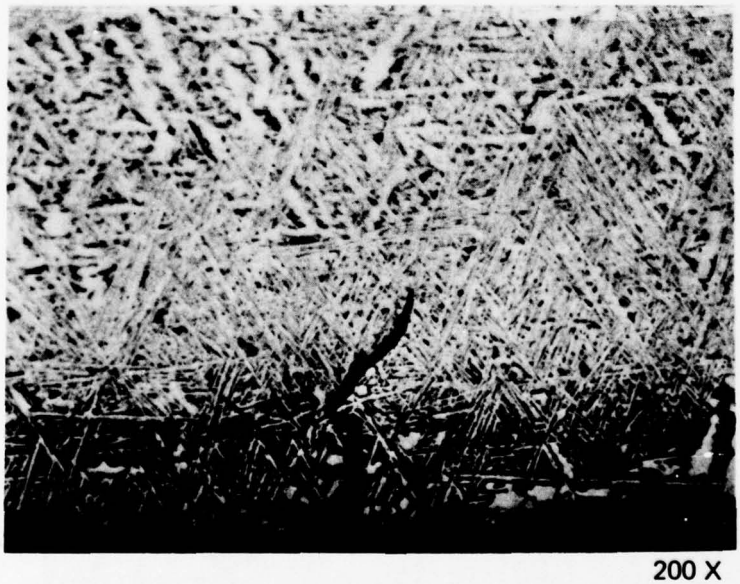

200 X

b. Profile of crack seen on longitudinal section. Vertical section through the crack shown in a above. The tip of the arrow lies on the bonded crack, which is an extension of the slanted lower portion of the open crack.

FIGURE 24. CONFIGURATION OF PARTIALLY BONDED CRACK LOCATED IN THE REGION SHOWN IN FIGURE 23

The surface layer is nickel not completely removed after HIP.

a. Etched surface 1000 X

b. Etched surface partially polished 1000 X

FIGURE 25. SHOWS DETAIL OF PARTIALLY BONDED CRACK INDICATED BY THE ROW OF POROSITY REMAINING AFTER INCOMPLETE BONDING

The layer is nickel not completely removed after HIP.

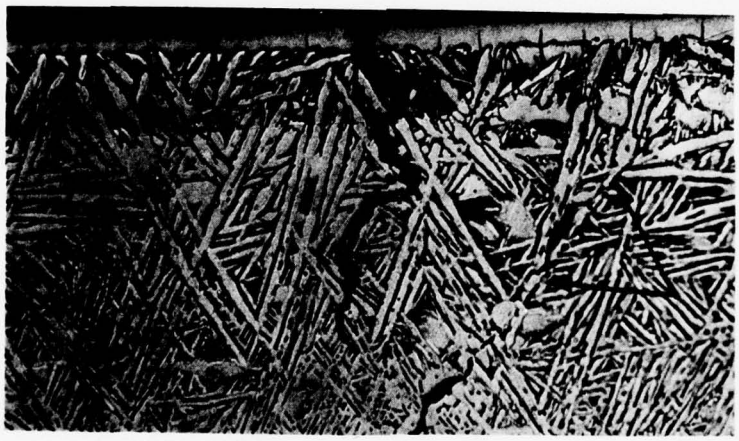

500 X

FIGURE 26. SAME CRACKS AS SHOWN IN FIGURES 24 AND 25 AFTER REMOVING 0.5 mm FROM METALLOGRAPHIC SURFACE

The region of the partially bonded crack at the tip of the arrow is de-focused slightly to show up the porosity better.

diffusion zone where nickel has diffused down into the alloy substrate during the HIP cycle. This diffusion zone proves the intimate contact between the nickel plate and alloy substrate in this region which promoted the closure and bonding of the initial crack. In other regions and on other specimens, no diffusion zone was present. In these instances, the coating-substrate contact was poor during HIP, indicating that no sealing of the surface cracks in the specimens substrate from the HIP atmosphere could have been achieved.

The nickel layer (Figures 25 and 26) contains numerous cracks normal to the surface extending completely through the nickel layer. These are potential crack initiation sites, and the crack in Figure 26 presumably started at one of these. Also the nickel diffusion zone probably has quite different fatigue properties compared to Ti-6Al-4V. Being at the surface, this zone could strongly influence the final fatigue properties. In one sense at least, crack initiation is different in this layer than in Ti-6Al-4V. The crack appears to enter Stage II very near the surface and propagates through the particles of the light phase (probably α) rather than along interphase boundaries as observed in Ti-6Al-4V.

Finally, HIP coarsened the microstructure as shown in Figure 27; compare to Figure 1. The thermal portion of the HIP cycle [3 hr at 843 C (1550 F), furnace cool] is well above the overage temperature, 732 C (1350 F). It has been reported that coarser structures show lower fatigue lives[9], but present rejuvenation results indicate that there is no decrease in life after HIP of undamaged specimens. Thus, the amount of coarsening occurring during HIP does not seem to significantly influence the fatigue life after HIP of undamaged specimens. However, other factors such as the morphology of the phases are also important in the complexity of microstructures in Ti alloys, and these could have offsetting effects which cannot be separated here.

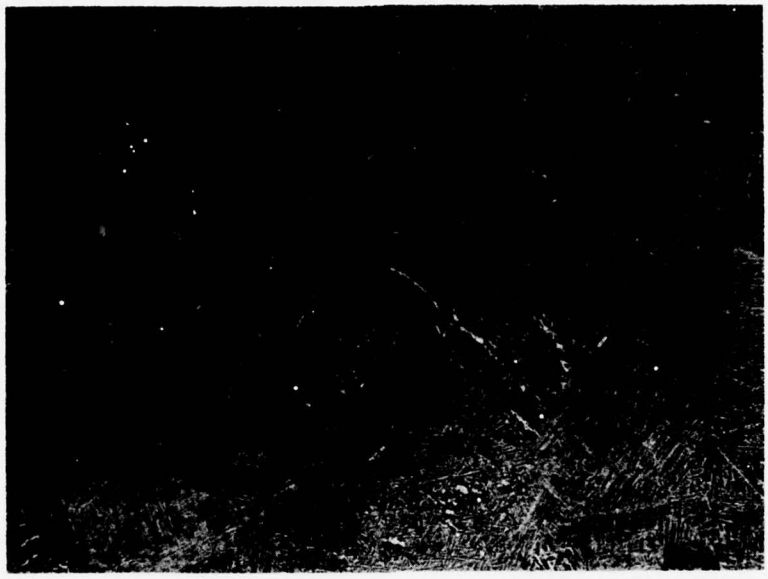

a. 50 X

b. 500 X

FIGURE 27. MICROSTRUCTURE OF Ti-6Al-4V IN THE βSTOA CONDITION AFTER HIP AT 843 C (1550 F) FOR 3 HOURS

COMMENTARY AND CONCLUSIONS

The interpretation and analysis of the data is hampered by the limited number of test specimens and amount of metallography that could be performed. This occurred in part because the purpose of this investigation was to determine the feasibility of HIP rejuvenation, and not to be a detailed study of mechanisms. Because of this, care is required to approach the data with a balanced perspective, and not place too much or too little weight on certain elements of the data. For example, the effects of variables such as plastic strain range do influence low cycle fatigue life and should be considered as part of the analysis, as well as total strain range. Also, even though the actual baseline data were limited to one specimen, sufficient other data were available to bracket this condition that a baseline behavior could be specified. Thus, reasonable confidence can be placed in the baseline comparisons.

The overall rejuvenation results showed improvements, although these were often modest. On the basis of total strain range, the effective percentage of maximum possible rejuvenation achieved was: Level 1 damage; H_1, 69 percent; $C_T + H_1$, 112 percent; and Level 2 damage, 32 to 60 percent (the latter including only these specimens which didn't fail at a visible pre-existing crack). On the basis of plastic strain range, the effective percentage of maximum possible rejuvenation achieved was: Level 1 damage, H_1, 15 percent; $C_T + H_1$, 33 percent; and Level 2 damage, 68 percent for failures not associated with previously mapped cracks.

These improvements were obtained using surface coatings, which to work best should be mechanically and chemically compatible with the Ti-6Al-4V specimens. Any degradation of properties through effects of the coatings such as lowering fatigue crack initiation life or non-adherance detracts from associated improvements in life. An example is the cracks in the residual nickel coating seen in Figures 25 and 26, one of which propagated into the nickel diffusion zone in the surface of the fatigue specimen.

The metallographic results showed that fatigue-induced surface cracks can be closed and there is strong evidence that closed cracks can be bonded. The requirements are that the cracks are completely bridged over and sealed, the crack surfaces are sufficiently clean that bonding is not inhibited, and the HIP parameters of time, temperature, and pressure are sufficient to affect closure and bonding during the HIP cycle. Failure to meet any one of these requirements can prevent crack closure and bonding.

The strictness of these requirements places a perspective on the present results. These results were achieved by using only one set of HIP parameters and Ti alloy coating parameters developed from only two trial runs. Thus the entire arena regarding the tradeoff between coating properties, crack closure and bonding versus microstructural effects of HIP remains to be

investigated to determine optimum HIP conditions. Various types, combinations and sequences of coatings should be explored to obtain an optimum coating for the rejuvenation process. From this point of view, the results are certainly encouraging, in showing that HIP rejuvenation is feasible and that through optimization of the process parameters, larger improvements should be expected.

RECOMMENDATIONS

It is clear that the initial assessment of the coating being the most critical area at this stage was borne out by the results of this program. Also, although cleaning of the damaged surface was not a factor in this program, the importance of the coating emphasizes the importance of surface preparation and cleaning in any application where surface compounds and dirt are present after service. Therefore, the principal recommendation is to pursue development in cleaning and coating techniques applicable to Ti-6Al-4V disks. The cleaning techniques must remove unwanted compounds from both the part surface and also from within the cracks. In titanium alloys it may not be necessary to remove small amounts of oxide from within the cracks if they are dissolved in the metal metrix during subsequent HIP rejuvenation. Coatings may be of two types. A permanent coating must be compatible chemically and mechanically to the substrate material. A sacrificial coating must be non-interacting with the substrate, bonded well at the HIP temperature, and easily removable after HIP. Both types of coating must bridge the largest cracks allowable by inspection and be amenable to coating difficult to reach regions on a disk, e.g., inside dovetails and bolt holes. A permanent coating may be required to neutralize that portion of Level 1 damage associated with surface offsets or slip steps.

APPENDIX A

FATIGUE RESULTS FOR MILL-ANNEALED Ti-6Al-4V

APPENDIX A

FATIGUE RESULTS FOR MILL-ANNEALED Ti-6Al-4V

This appendix details the results of tensile and fatigue tests to develop baseline data for M/A Ti-6Al-4V. Results obtained from the duplicate tensile bars (Specimens 6 and 7) were typical of mill-annealed material. Several fatigue tests were performed in fully reversed strain control at a variety of strain levels ranging from ± 2.0 percent to ± 0.46 percent to establish the strain-life behavior of the mill-annealed material. Data so obtained (Specimens 3 to 11, reported in Table 10), indicated that subsequent testing at a total strain range of about 0.92 percent was possibly suitable as the strain amplitude for all subsequent testing. Because the metal's deformation response was elastic at this strain range, the first of the tests to document the life scatter at the selected test amplitude was performed in load control at a load level selected to match the stress response observed in strain control. Likewise, the second test of this series was performed in load control. For strain controlled tests, the life to crack initiation, N_i, was defined as the number of cycles until an asymmetric decrease in the tensile load of 5% from the stable value reached during the fatigue test occurs. (Load was monitored continuously during the strain control tests.)

Results of all the fatigue tests show that, for this mill-annealed material, the life spent initiating a crack large enough to cause a 5 percent load drop (or a displacement change in load control equivalent to a 5 percent drop) occupied a very large fraction of the total life. As evident from a study of Table 10, this fraction was greater than 95 percent of the total life in the range of lives of interest in this program (10^3 to 10^5 cycles). Studies of surface damage using surface replication techniques reinforce these observations; even after 95 percent of the life was expended, no surface cracks were seen. These results confirm those reported by Wells and Sullivan[10]. These findings, coupled with the scatter observed for Specimens 11, 12, and 13 suggested that the planned examination of post-initiation predamage in subsequent steps of the program would have proved difficult at best. Without this post initiation case, it would not be possible to demonstrate the healing effects of coating and HIP on documented surface damage such as micro-cracks.

Therefore, the mill annealed material was given a series of alternative heat treatments to identify a heat treated condition which would provide a crack initiation life on the order of 0.8 or less of the separation life. The attainment of this objective was necessary to enable a study of the feasibility of HIP rejuvenation of cracked fatigue specimens.

TABLE 10. RESULTS OF TESTS ON MILL-ANNEALED Ti-6Al-4V

Specimen No.	Δe^T percent	ΔS[a] ksi	N_5[b] Cycles	N_f Cycles	N_5/N_f percent
6	(d)				
7	(d)				
4	2.04	243.60	1,608	1,608	100
5	4.14	233.00	110	122	90.2
3	1.0	–	–	405[c]	–
8	2.03	216.40	1,775	1,797	98.8
9	1.49	204.6	3,275	3,511	93.3
10	1.10	196.10	15,500	15,651	96.9
11	0.92	167.70	87,100	87,400	99.7
12	0.92	167.20	58,820	59,010	99.7
13	0.92	167.20	65,874	65,821	98.9
16	0.92	167.60	–	>39,500[c]	–

(a) Stress at $N_f/2$.

(b) Number of cycles at a 5 percent drop in load or its equivalent in terms of displacement.

(c) Test terminated prematurely.

(d) Specimens used for tensile testing.

APPENDIX B

INVESTIGATION OF ALTERNATIVE HEAT TREATMENTS FOR MILL-ANNEALED Ti-6Al-4V

APPENDIX B

INVESTIGATION OF ALTERNATIVE HEAT TREATMENTS FOR MILL-ANNEALED Ti-6Al-4V

Since the mill-annealed condition did not have a suitable crack propagation interval, it was decided that a microstructural modification by heat treatment might provide the combination of toughness and resistance to crack propagation required to provide sub-critical size surface cracks. Other heat treatments have been reported to give improved fatigue life compared to the mill-annealed condition.[9] Although the reasons for the variation in fatigue life between these conditions is not resolved, it appears that refinement of the α and β constituents plays an important role. Each of the five heat treatments presents variations of microstructure refinement compared to the mill-annealed condition.

Another point of conjecture is the part of the fatigue process in which the benefits of these heat treatments is realized. It is often reported that the microstructure has very little effect on the crack propagation behavior, since notched specimens don't show much difference in life for different heat treatments whereas smooth bar results do. If this were true, then supposedly the crack propagation period could not be expanded sufficiently to enable cracked fatigue specimens to be consistently obtained, similar to the problem in mill-annealed material. However, this was not so.

The five heat treatments presented below were selected as those which would provide a broad range of toughness and fatigue life for this alloy.

(1) β-anneal: 1038 C (1900 F), 1 hr, air cool.

(2) Duplex β anneal: 1038 C (1900 F), ½ hr, air cool + 704 C (1300 F), 4 hr, air cool.

(3) Solution Treat and Age (STA): 949 C (1740 F), 1 hr, water quench + 538 C (1000 F), 4 hr, air cool.

(4) Solution Treat and Overage (STOA): 471 C (1780 F), 1 hr, water quench + 704 C (1300 F), 2 hr, air cool.

(5) Beta Solution Treat and Overage (βSTOA): 1010 C (1850 F), 1½ hr, water quench + 732 C (1350 F), 3 hr, air cool.

Thus, if it were possible to obtain a sufficiently long crack propagation stage in Ti-6Al-4V, there would be a good chance of discovering this fact by testing specimens in these conditions. One specimen for each heat treatment was used. It was expected that any significant result would be observed even in a single test.

After heat treatment*, 2 of the 5 specimens were cycled to failure in strain control at a total strain range of 1.25 percent. The remainder were tested in load control at a load level nominally corresponding to a cyclic stress range of 167.6 ksi based on the uncracked minimum section. The results are tabulated in Table 11. Instead of the standard surface preparation used in this program, the specimens given heat treatments (3) - (5) were electropolished and etched as discussed later. The overall results (Table 11) show that heat treatments (4) and (5) showed promise of increased crack propagation interval. Therefore, duplicate specimens were prepared for the STOA and βSTOA conditions. These specimens (40-43) were cycled at a constant strain range of 0.98 percent. Specimens 40 and 41, which received the βSTOA treatment, failed at 25,000 and 23,770 cycles, respectively. Based on extrapolated load-time data, crack initiation occurred at 22,000 and 21,200 cycles, respectively. The corresponding values of the fraction N_i/N_f are 0.88 and 0.89. Specimens 42 and 43 received the STOA treatment. Based on extrapolated load-time response, crack initiation occurred at 26,100 and 23,350 cycles while separation occurred at 27,880 and 26,740 cycles, respectively, for Specimens 42 and 43. The corresponding values of the fraction N_i/N_f for these data are 0.94 and 0.95.

Based on these data and a consideration of the program's objectives, the βSTOA treatment was selected as the baseline material condition for the remainder of the program. Heat treating and the machining of additional specimens (to replace those used in the exploratory heat treatment study reported here) has been discussed in the text.

In addition to the mechanical methods of detecting crack initiation discussed earlier, metallographic inspection of the surface was also used. To relate any surface cracking to microstructural features, the surface of the fatigue specimens were electropolished and etched before the fatigue test as done by Wells and Sullivan[10]. The tests were stopped, held at zero load, and surface replicas made at intervals of 5,000 to 10,000 cycles. These replicas were then examined at magnifications up to 10,000 diameters in an electron microscope. Specimens given heat treatments (3) to (5) were examined in this way.

The STA condition had no visible surface cracks even after failure. The STOA condition had some very small ($\sim 1\ \mu$ long) surface cracks at 80 percent of the fatigue life, but these were rare, even after failure. The βSTOA condition had a short life compared to the other conditions indicating possible premature failure. No surface cracks were observed either after 85 percent of the final life or after failure. The absence of surface cracks in these specimens after failure suggested that crack initiation was a singular event when it occurred and this initial crack must propagate rapidly. A possible rationale for this behavior is that the first crack was prematurely initiated and propagated to failure before the actual crack initiation life,

* The specimens were heat treated after machining to fatigue specimens.

TABLE 11. RESULTS OF FATIGUE TESTS ON HEAT-TREATED SPECIMENS

Specimen Number	Stress Range ksi	N_i/N_f percent	N_f Cycles	Heat Treatment[a]
49	106.8[b]	~ 100	3,085	(2) Duplex β anneal
48	212.6[b]	~ 100	2,307	(1) β anneal
47	167.6[b]	–	32,714[e]	Mill anneal[c]
46	167.6	~ 100	52,454	(3) STA
45	167.6	90	48,017	(4) STOA
44	167.6	94	23,992	(5) βSTOA
43	164.40[d]	95	26,740	(4) STOA
42	162.6[d]	94	27,880	(4) STOA
41	167.1[d]	89	23,770	(5) βSTOA
40	162.8[d]	88	25,000	(5) βSTOA

(a) Numbers refer to code introduced earlier in this appendix.
(b) Tests performed in strain control at a range of 1.25 percent.
(c) Mill annealed, but electropolished for use in replication studies.
(d) Tests performed in strain control at a range of 0.98 percent.
(e) Failed at gage length/shoulder fillet transition -- no valid indication of initiation available.

representative of smooth bars, was reached. Even so, the length of the propagation period measured in Table 11 was encouraging.

As noted previously, the results obtained for heat treatments (4) and (5) were supplemented by further testing and replication; a total of four specimens being used. Replicas of the surface of each of the four fatigue specimens were made at intervals during the fatigue testing. Specimen 40 (βSTOA heat treatment) was replicated at 5000-cycle intervals, while each of the others was replicated at 4000-cycle intervals. All replications were made without removing the specimen from the fatigue machine and a 7500-lb tensile load was applied to the specimens during replication.

Replicas taken in the vicinity of the fracture were examined extensively for the conditions just before and after fracture. No features which could be unambiguously identified as cracks were observed on any of the specimens. In one case, the crack leading to final fracture was found during the examination for replication just preceding failure and a replica was made in the vicinity of this crack. This region was no different from the others.

Thus, extensive easily observed surface cracking apparently is not formed during fatigue of either the STOA or βSTOA conditions at a strain range of 0.98 percent. Surface fatigue cracks other than the one leading to failure probably exist in the surface of each specimen, but they are relatively few in number and require extensive searching using surface replication techniques.

A possible source of premature crack initiation were the notches created at the etched interfaces between the microstructural phases. This possibility was tested in a mill-annealed material by electropolishing and etching Specimen 47 and testing it at a total strain range of 0.92. This specimen had a life of 32,712 cycles compared to lives of 65,821 to 87,400 cycles for specimens having mechanically polished surfaces (Table 10), but it was an invalid shoulder failure so the comparison is not definitive. Also, comparison of the STOA and βSTOA specimens having mechanically polished surfaces (Specimens 40-43) to those having etched surfaces (Specimens 44 and 45) show no difference between the two conditions.

From these results the βSTOA heat treatment with mechanically polished surfaces (even for metallographic damage characterization specimens) was selected as an appropriate condition to investigate the feasibility of fatigue rejuvenation in Ti-6Al-4V alloy.

APPENDIX C

INVESTIGATION OF HIP TEMPERATURE EFFECTS ON MICROSTRUCTURE OF MILL-ANNEALED Ti-6Al-4V BAR

APPENDIX C

INVESTIGATION OF HIP TEMPERATURE EFFECTS ON MICROSTRUCTURE OF MILL-ANNEALED Ti-6Al-4V BAR

It was initially planned that the mill-annealed condition of as-received Ti-6Al-4V bar would serve as the baseline condition for the rejuvenation by HIP investigation. Since the structure, and properties, of Ti-6Al-4V are extremely sensitive to thermal history, a preliminary investigation of the microstructural effects of possible HIP time-temperature combinations was conducted. As shown in Figure 28, the as-received material had a fine-grained alpha structure with some intergranular beta. The structure was equiaxed in the transverse direction and somewhat elongated in the longitudinal or rolling direction. A heat treatment at 954 C (1750 F) for 1 hour, a condition commonly used for powder consolidation and casting desification by HIP, caused considerable coarsening of the grain structure and the elongated grains became equiaxed as shown in Figure 29. As this thermal treatment and resultant structural change would, in itself, cause significant changes in fatigue properties, severe HIP thermal treatments were investigated. As shown in Figures 30 to 32, thermal treatments including 4 hr at 760 C (1400 F), 3 hr at 815 C (1500 F), and 2 hr at 870 C (1600 F) had little effect on the microstructure except for some slight decrease in longitudinal grain anistropy. Thus, to minimize microstructural coarsening, the HIP conditions should be limited to temperatures below 870 C (1600 F) and times of a few hours.

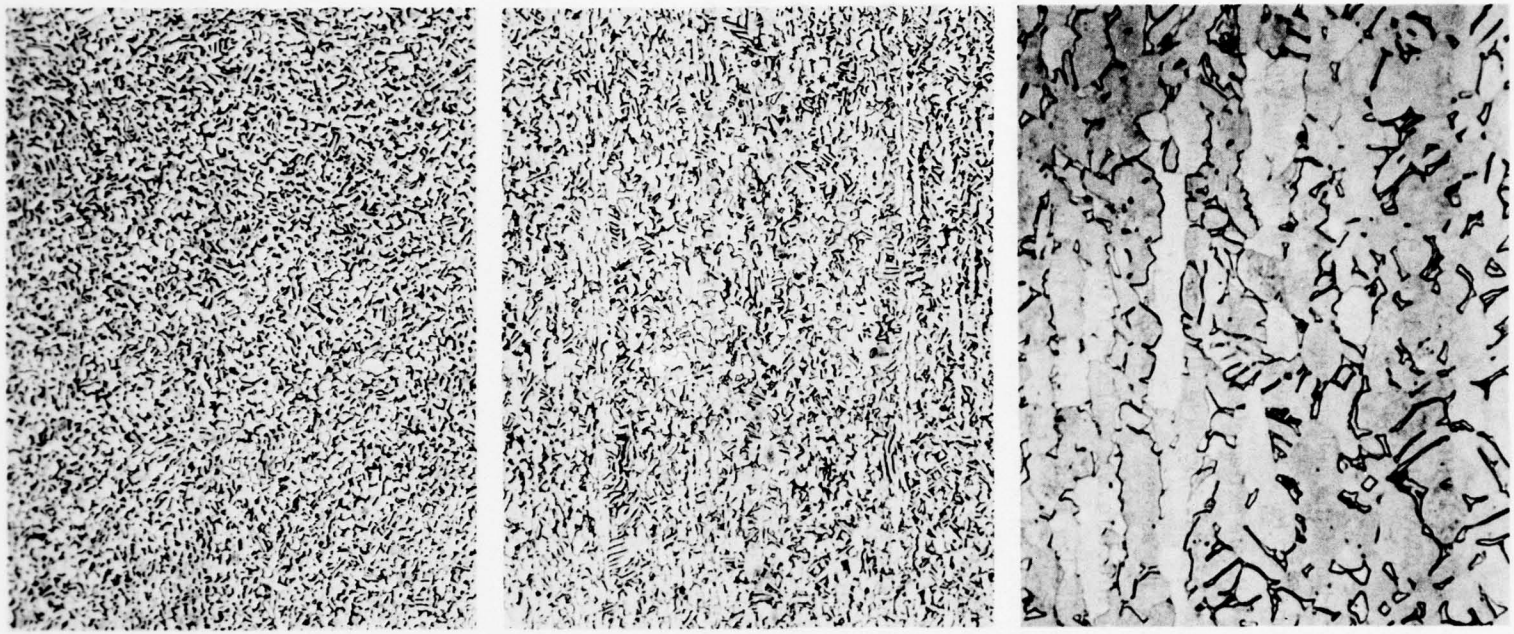

a. Transverse Section 250 X b. Longitudinal Section 250 X c. Longitudinal Section 1000 X

FIGURE 28. MICROSTRUCTURE OF Ti-6Al-4V BAR AS-RECEIVED IN THE MILL-ANNEALED CONDITION

The bar axis is vertical in the micrographs.

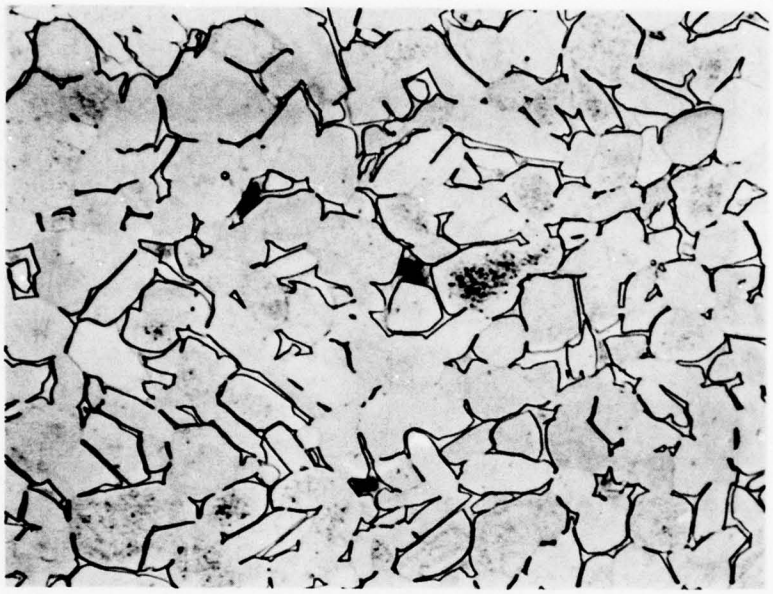

1000 X

a.

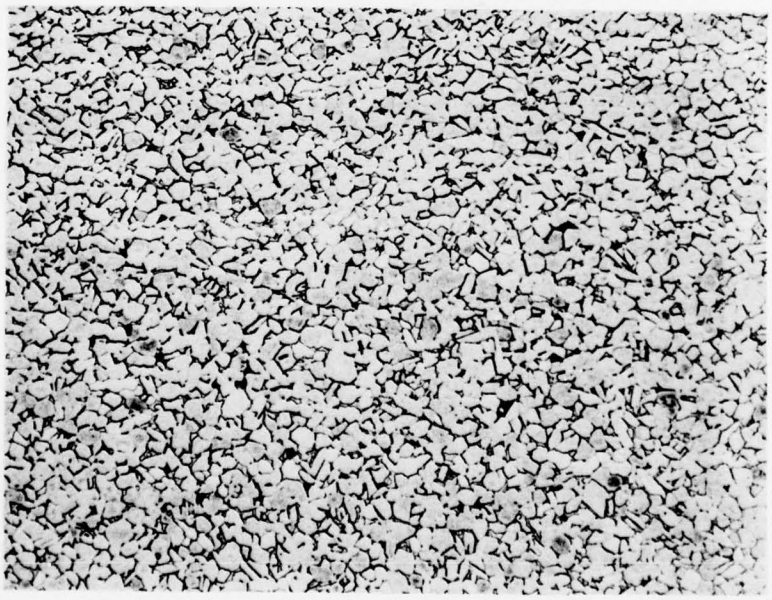

250 X

b.

FIGURE 29. MICROSTRUCTURE OF Ti-6Al-4V BAR AFTER 954 C (1700 F), 1 HOUR, LONGITUDINAL SECTION WITH LONGITUDINAL AXIS HORIZONTAL

1000 X

a.

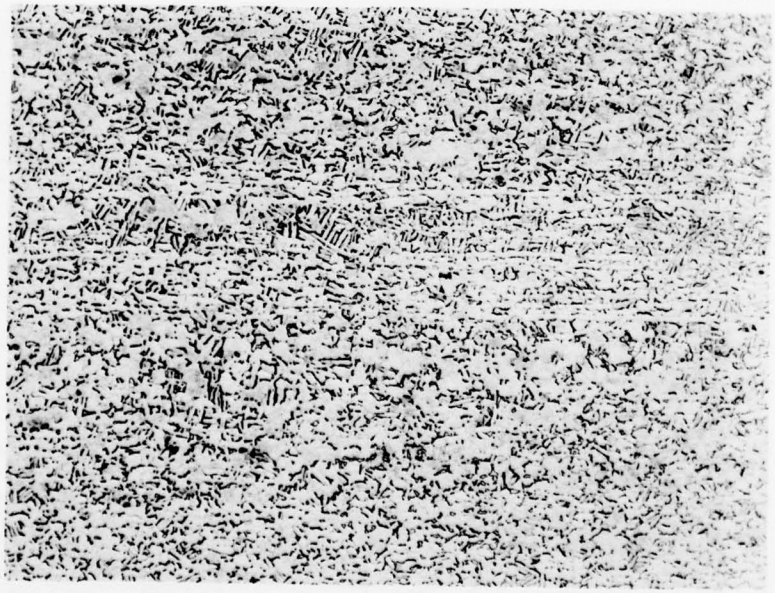

250 X

b.

FIGURE 30. MICROSTRUCTURE OF Ti-6Al-4V BAR AFTER HEAT TREATMENT OF 760 C (1400 F), 4 HOURS, LONGITUDINAL SECTION

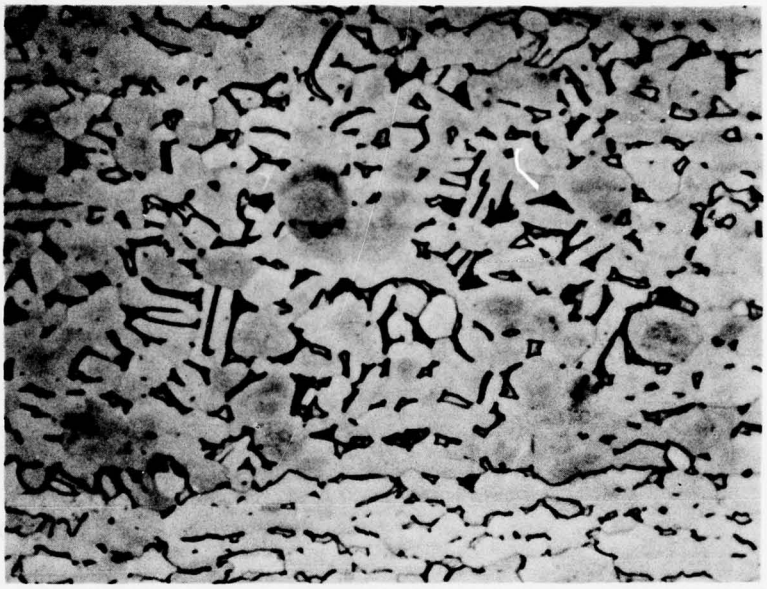

1000 X

a.

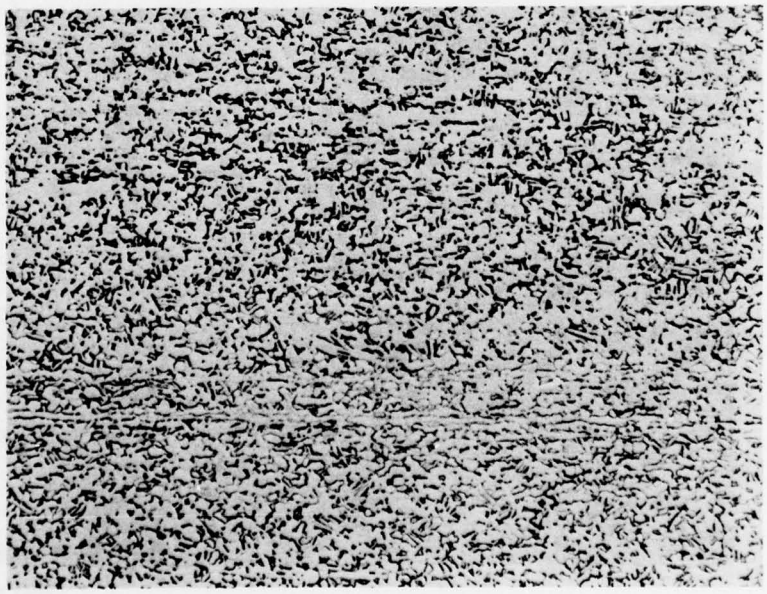

250 X

b.

FIGURE 31. MICROSTRUCTURE OF Ti-6Al-4V BAR AFTER HEAT TREATMENT OF 815 C (1500 F), 3 HOURS, LONGITUDINAL SECTION

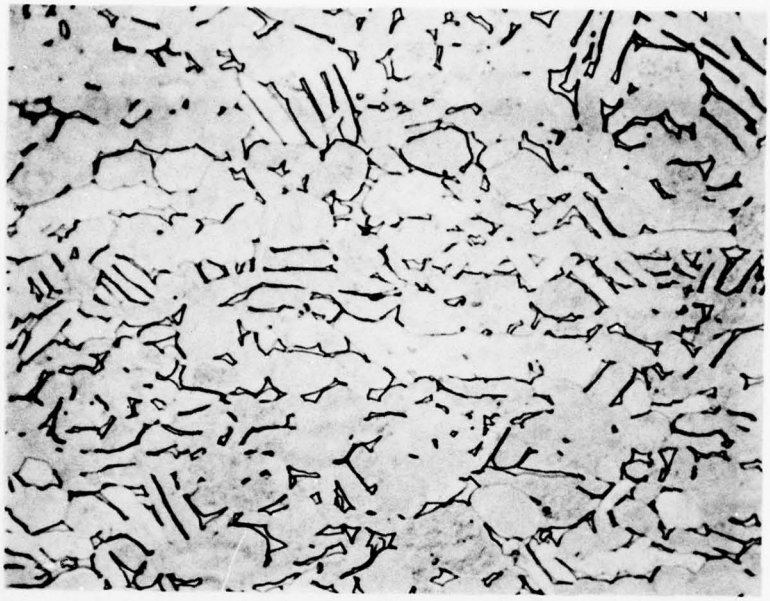

1000 X

a.

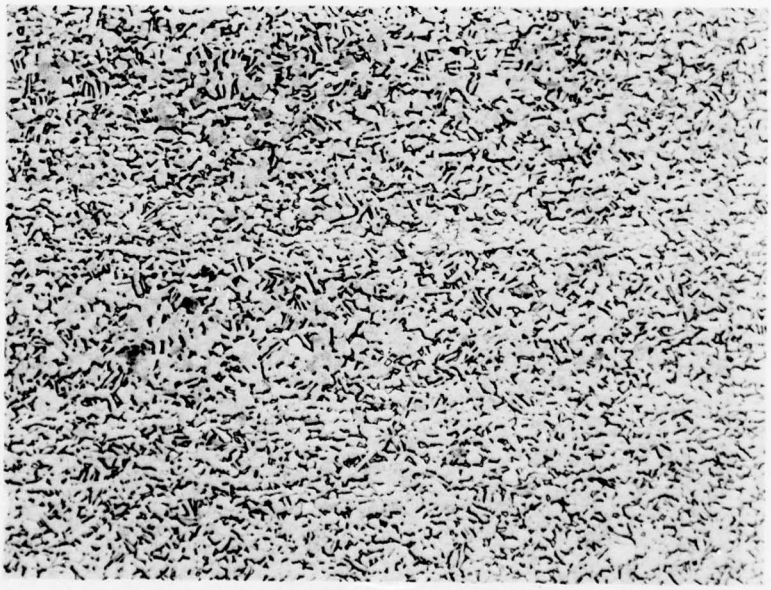

250 X

b.

FIGURE 32. MICROSTRUCTURE OF Ti-6Al-4V BAR AFTER HEAT TREATMENT OF 870 C (1600 F), 2 HOURS, LONGITUDINAL SECTION

APPENDIX D

STUDY OF THE INFLUENCE OF COATING PARAMETERS, SHOT PEENING AND HEAT TREATMENTS ON THE Ti-6Al-4V COATINGS

APPENDIX D

STUDY OF THE INFLUENCE OF COATING PARAMETERS, SHOT PEENING AND HEAT TREATMENTS ON THE Ti-6Al-4V COATINGS

The structural morphology and hardness of permanent coatings used to bridge surface cracks and defects can have a significant effect on the fatigue properties of the study material. Therefore, an investigation was conducted to study the effect of various combinations of thermal treatments and shot peening on the microstructure and hardness of the electron beam evaporated coatings.

Thirty disks (coupons) 1/8-inch thick were sliced from the Ti-6Al-4V rod. After metallographic grinding of one face of each coupon to a surface finish of about 10 microinches, the ground surface of twelve coupons was shot peened to create surface roughening indicative of possible pretreatments that may be required of components removed from service. Clean glass shot (beads) 0.020 to 0.030 in. in diameter were used for this treatment. All thirty disks were then coated on the shot peened or ground surface with a 0.002- to 0.004-inch thick coating from the Ti-7.04Al-4.74V electron beam source ingot. These coupons were coated in two runs of 15 coupons each.

A typical cross section of the coated specimens is shown in Figure 33. The coatings would have a duplex microstructure consisting of $\alpha + \beta$ with the relative amounts of each phase depending on the variation of Al and V through the coating thickness.

The influence of shot peening and heat treatment on coating microstructure, hardness, and bonding to the substrate was investigated. Coated specimens having peened and ground substrate surfaces were heat treated at 704 C (1299 F) for 3 hours (mill anneal) and examined (Figure 34). The overall effect of this treatment was to significantly increase the coating grain size and initiate diffusion bonding of the coating to the substrate as shown by comparison of Figure 34 with Figure 33.

Coated specimens peened at 20, 40, and 55 psi driving air pressure were sectioned and subjected to Knoop microhardness testing along with an unpeened coupon. As indicated in Table 12, overall coating hardness appeared to increase with peening intensity. Unfortunately, structural differences between the coated specimens may have influenced these results. Two additional coated coupons, one peened prior to coating, were therefore cut in half for further peening experiments. After peening one-half of each coupon, microhardness comparisons were again made. Knoop indent measurements across the coating thicknesses and into the substrate material indicated that the effect of peening was minimal. Erratic variations in hardness were

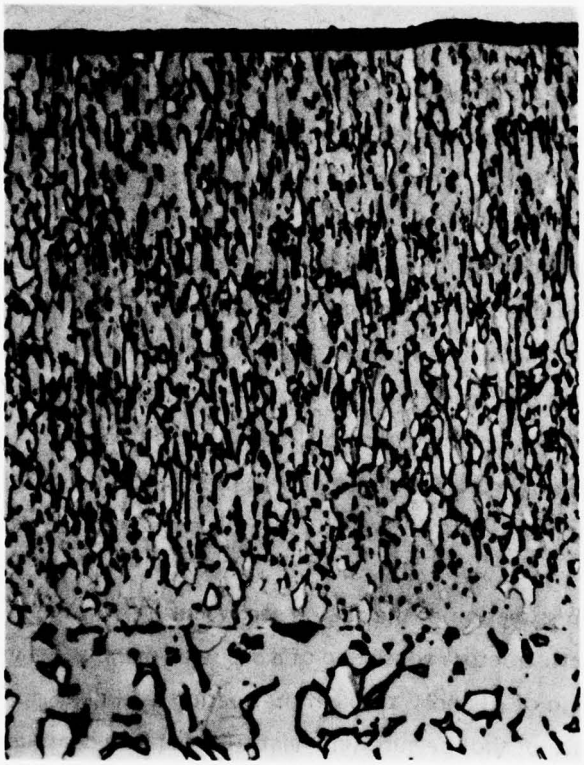

1000 X

FIGURE 33. Ti-Al-V COATING MICROSTRUCTURE IN THE AS-DEPOSITED CONDITION

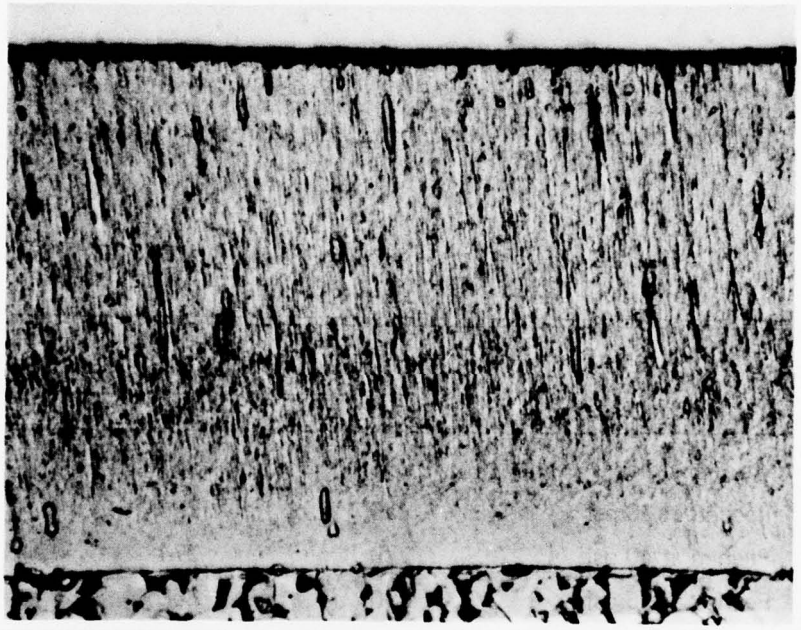

1000 X

FIGURE 34. Ti-Al-V COATING MICROSTRUCTURE AFTER 704 C (1299 F), 3 HOUR VACUUM ANNEAL, 300 C/HOUR FURNACE COOL

TABLE 12. EFFECT OF SHOT PEENING INTENSITY ON COATING HARDNESS

Coating Condition	Knoop Hardness, 500 g load		
	Max	Min	Avg
As-deposited	265	250	255
Peened at 20 psi	265	250	259
Peened at 40 psi	279	274	276
Peened at 55 psi	290	263	277

observed for all four specimens as the coating thickness was traversed. These are attributed to variations in the aluminum content of the coatings rather than the effects of peening.

The effects of peening and HIP on coating morphology were investigated using a single coated disk cut into three pieces. Two of these segments, one of which was shot peened, were vacuum heat treated at 815 C (1500 F) for 3 hours with slow cooling to simulate the temperature profile of a possible HIP treatment. The third segment was left in the as-coated condition. Metallographic examination of these segments showed that the fine columnar structure of the as-deposited coating (Figure 33) coarsened to an elongated α-β microstructure similar to that of the mill-annealed substrate, (Figure 35). Peening prior to HIP, a possible treatment to force the coating into surface cracks, appears to cause a thin (approximately one grain) recrystallized layer to form on the coating surface. Also, there is some indication in Figure 35a and 35b that the substrate coating interface is more diffuse and therefore better bonded after shot peening.

The HIP cycle and possibly shot peening of the coating, could aid in homogenizing the vanadium and aluminum content in the coating. The three-segment disk discussed above was analyzed in the electron microprobe for aluminum and vanadium distribution through the coating and into the adjacent substrate. The vanadium content remained approximately constant throughout the coating and substrate of all three disk segments but was much more uniformly distributed in the as-deposited coating than in the substrate material. After heat treating, however, the vanadium distribution in the deposited film could not be distinguished from that in the substrate. Distribution of the aluminum in the deposited film is illustrated by the smoothed curves in Figure 36; high at the coating-substrate interface and low throughout the remainder of the coating. The heat treatment at 815 C (1500 F) smoothed out local irregularities in the distribution and the shot peening did not add to this effect.

AD-A053 289 BATTELLE COLUMBUS LABS OHIO F/G 11/6
INVESTIGATION OF REJUVENATION OF FATIGUE DAMAGE IN TI-6AL-4V.(U)
JUL 77 A H CLAUER, B N LEIS, R B LOVE F33615-76-C-5100
UNCLASSIFIED AFML-TR-77-107 NL

2 OF 2
AD
A053289

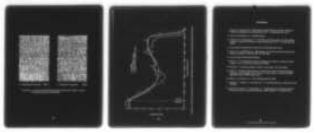

END
DATE
FILMED
6-78
DDC

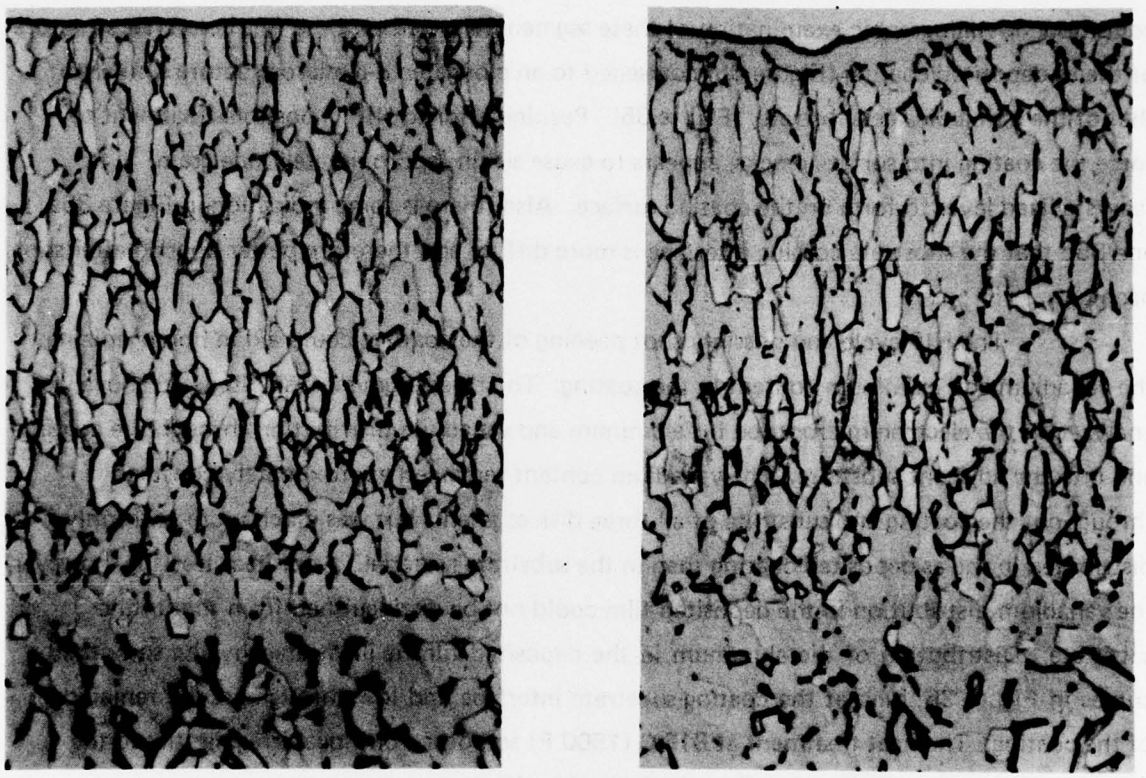

a. As-deposited & heat treated 1000 X

b. Peened prior to heat treat 1000 X

FIGURE 35. Ti-Al-V COATING MICROSTRUCTURE AFTER 815 C (1500 F), 3 HOUR, HIP SIMULATION HEAT TREATMENT

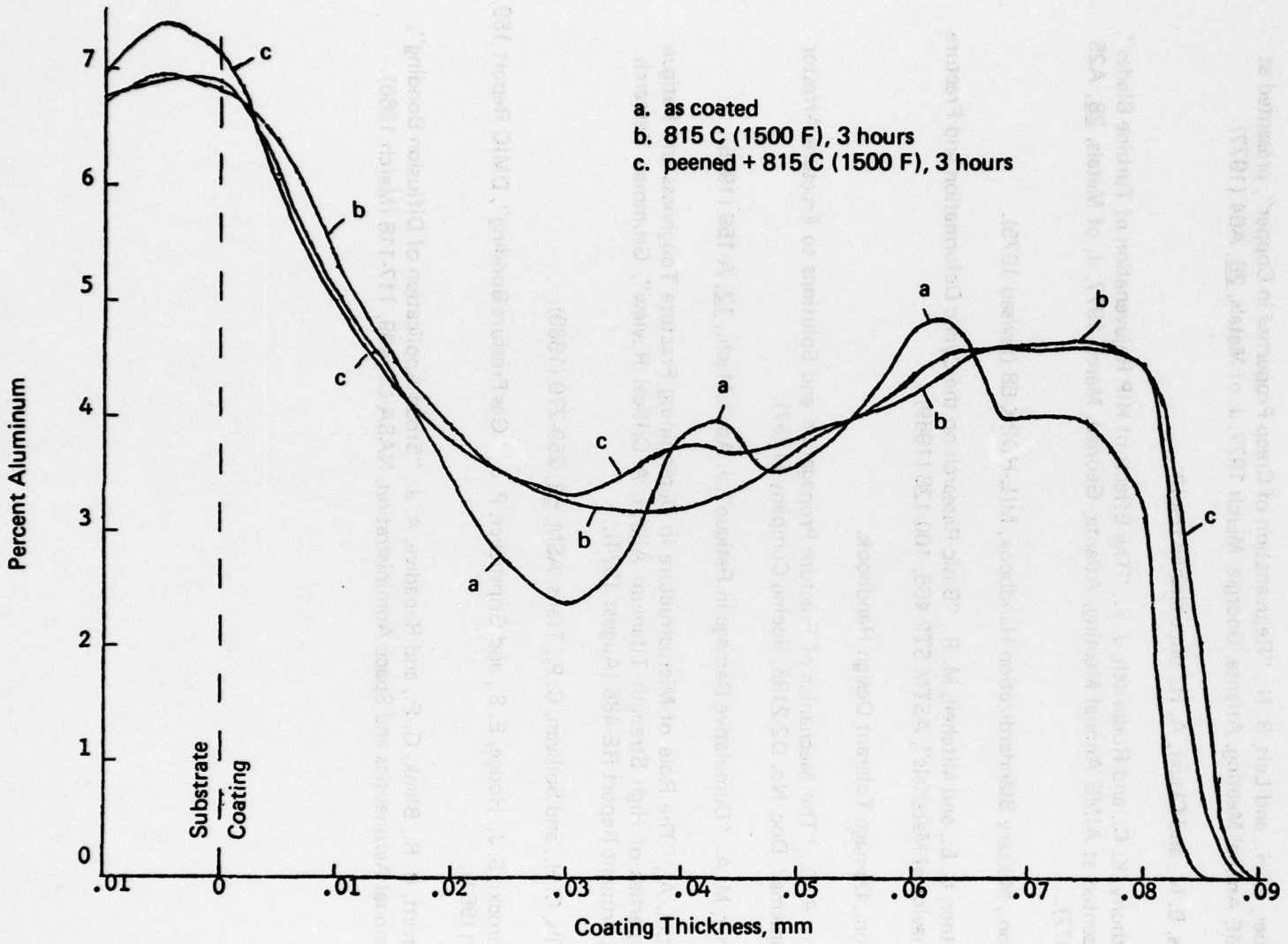

FIGURE 36. EFFECT OF PEENING AND HEAT TREATMENT ON SMOOTHED ALUMINUM MICROPROBE PROFILES

REFERENCES

1. Clauer, A. H., and Leis, B. N., "Rejuvenation of Creep Properties in Copper", presented at AIME Annual Meeting, Atlanta, Georgia, March 1977, J. of Metals, 28, A64 (1977).

2. Leis, B. N., and Clauer, A. H., unpublished results.

3. Anthony, K. C., and Rodavitch, J. F., "The Effects of HIP Rejuvenation of Turbine Blades", presented at AIME Annual Meeting, Atlanta, Georgia, March 1977, J. of Metals, 28, A25 (1977).

4. Anon., Military Standardization Handbook, MIL-HDBK-58 (revised 1975).

5. Feltner, C. E., and Mitchell, M. R., "Basic Research on the Cyclic Deformation and Fracture Behavior of Materials", ASTM STP 465, 100-128 (1969).

6. Anon., Damage Tolerant Design Handbook.

7. Paris, P. C., "The Mechanics of Fracture Propagation and Solutions to Fracture Arrestor Problems", Doc. No. D2-2195, Boeing Company (1957).

8. Miner, M. A., "Cumulative Damage in Fatigue", J. Appl. Mech., 12, A-159 (1945).

9. Tobin, A., "The Role of Microstructure in Determining Fracture Toughness and Fatigue Properties of High Strength Titanium Alloys, A Critical Review", Grumman Research Department Report RE-485 (August 1974).

10. Wells, C. H., and Sullivan, C. P., Trans. ASM, 62, 263-270 (1969).

11. Paprocki, S. J., Hodge, E. S., and Gripshover, P. J., "Gas Pressure Bonding", DMIC Report 159, 12 (1961).

12. Garrett, B. R., Blank, G. F., and Ranadive, A. J., "Broad Application of Diffusion Bonding", National Aeronautics and Space Administration, NASA CR-409, 117-118 (March 1966).

*U.S.Government Printing Office: 1978 — 757-080/315